Advanced Composites and Hybrid Materials (2025) 8:366
https://doi.org/10.1007/s42114-025-01466-z

RESEARCH

Half-metallicity and spin-gapless semiconducting properties in FeCrTiM (M = Al, As, Si) quaternary heusler alloys for spintronic, thermoelectric and optoelectronic applications

R. Ameur[1] · K. Bouferrache[2,3] · A. Guibadj[1] · M. A. Ghebouli[2,4] · B. Ghebouli[5] · M. Fatmi[2] · Faisal Katib Alanazi[6]

Received: 24 May 2025 / Revised: 27 August 2025 / Accepted: 4 September 2025

Abstract
The structural, electronic, magnetic, thermal, and optical properties of the quaternary Heusler alloys FeCrTiM (where M = Al, As, Si) were investigated using first-principles density functional theory (DFT) calculations. The ground state is found to be the type-1 ferrimagnetic configuration. In addition, the calculated formation energies (− 1.63 eV for FeCrTiAl, − 1.048 eV for FeCrTiAs, and − 0.774 eV for FeCrTiSi) confirm that these compounds are thermodynamically stable relative to their elemental constituents**,** suggesting the possibility of experimental synthesis under suitable conditions. The calculated lattice constants and ground-state parameters for FeCrTiAs and FeCrTiAl are presented as theoretical predictions. Based on band structure analysis, FeCrTiAs and FeCrTiSi exhibit half-metallic ferrimagnetism at equilibrium, although near spin-gapless features may emerge under lattice distortions. This makes them promising candidates for spintronic applications. All studied compounds display half-metallic ferrimagnetism with total magnetic moments that follow the Slater-Pauling rule, increasing linearly with the number of valence electrons. The optical properties reveal high static dielectric constants and refractive indices, indicating potential applications in optoelectronic devices. Additionally, the thermoelectric performance of these materials was evaluated, with calculated Seebeck coefficients up to ~ 1.5 $mV \cdot K^{-1}$, electrical conductivity $\sigma \approx 3.5 \times 10^6$ $S \cdot m^{-1}$, electronic thermal conductivity around 25 $W \cdot m^{-1} \cdot K^{-1}$, and a predicted figure of merit (ZT) close to 1 at 300 K. These combined results suggest that FeCrTiM (M = Al, As, Si) alloys are multifunctional materials with strong potential for use in high-performance energy conversion, optoelectronics, and spintronic devices.

Keywords Ab-initio · DFT · Structural characterization · Electronic properties · Thermoelectric · Optic

1 Introduction

Heuslers complex materials have recently become a hot topic after their discovery by Fredrich Heusler [1, 2]. Ab initio electronic structure calculations on the intermetallic quaternary Heusler XYZM, where X, Y and Z are transition or lighter transition metals and M is a III, IV and V groups elements, having 1:1:1:1 stoichiometry, called LiMgPdSn-type (also known as LiMgPdSb-type) as prototype material quaternary Heusler [3]. The valence of Y is lower than the valence of X atoms, and the valence of the Z element is lower than the valence of both X and Y. The sequence of the atoms along the fcc cube's diagonal is X–Y-Z-M (type 1), X-M-Y–Z (type 2) and X–Y-M-Z (type 3), where the first one is energetically the most stable [4]. These quaternary Heusler obey the Slater-Pauling rule with electronic and magnetic characteristics, which satisfy the half-metals, the

✉ M. Fatmi
fatmimessaoud@yahoo.fr

1 Laboratory of Materials Physico-Chemistry, University of Amar Telidji, BP 37G, 03000 Laghouat, Algeria

2 Research Unit On Emerging Materials (RUEM), University Ferhat Abbas of Setif 1, 19000 Setif, Algeria

3 Department of Physics, Faculty of Sciences, University of M'sila, University Pole, Road Bourdj Bou Arreiridj, 28000 M'sila, Algeria

4 Department of Chemistry, Faculty of Sciences, University of M'sila, University Pole, Road Bourdj Bou Arreiridj, 28000 M'sila, Algeria

5 Laboratory for the Study of Surfaces and Interfaces of Solid Materials (LESIMS), University Ferhat Abbas of Setif 1, 19000 Setif, Algeria

6 Department of Physics, College of Sciences, Northern Border University, 73222 Arar, Saudi Arabia

Published online: 01 October 2025

spin gapless semiconductors and semiconductors [3–5]. These compounds can be identified as ferrimagnetic or antiferromagnetic semiconductors, exhibiting a band gap that depends on the spin orientation. The magnetic ordering temperature corresponds to the Curie temperature for ferrimagnetic semiconductors and the Neel temperature for antiferromagnetic semiconductors [6]. Hence these Heusler alloys are studied because of their various magnetic phenomena. These Heusler alloys crystallize in a compact face centered cubic (fcc) structure having as a base four equidistant sites along a diagonal of the cube. Some of these Heusler are considered semi-metallic magnetic materials, as shown by the electronic band structure which is metallic in one of the spin directions, while it is semiconductor in the other leading to a spin polarization of the electrons at Fermi level. The calculation carried out by Lukashev et *al.* indicate that these materials undergo a band structure transition from a semimetallic phase at a small lattice constant to a near type 2 SGS in the ground state, then to a near type III SGS, and then to an SGS almost type I, when the lattice constant is increased [7]. In the SGS case, the maximum of the valence band and the minimum of the conduction band meet at the Fermi level and the electrons are excited from the valence band to the conduction band without or little energy. half-metallicity and spin-gapless semiconducting behavior is observed in FeCr-based quaternary Heusler [8]. Hebri et *al*. studied a series of lithium-based quaternary equiatomic Heusler in three different structural arrangements type1, type2 and type3 [9]. The quaternary intermetallic Heusler compounds CoFeMnZ (Z = Al, Ga, Si, or Ge) with 1: 1: 1: 1stoichiometry were synthesized using an arc-melting technique, exhibit half-metallic ferrimagnetism and analyzed using x-ray powder diffraction [10]. CoFeXSn (X = Ru, Zr, Hf, Ta) optimizing in three structural variants under ferrimagnetic ordering of spins and the result shows the ferrimagnetic phase is most stable [11]. The competition between austenitic and martensitic phases on equiatomic quaternary Heusler alloys ZnCdXMn (X = Pd, Ni, Pt), and their half-metallic behavior for the austenitic structure and 100% SP polarization traduced their useful in the spintronic devices uses [12]. One spin sub band of Half-metallic ferrimagnetic materials has a finite density of states at the Fermi level, the other sub band has a gap [13]. CoX′Y′Si, where X′ and Y′ are a transition metal with 4*d* electrons and either Fe or Mn shows half-metallic ferrimagnets with spin polarization nearly 100% with very high Curie temperatures [14]. FeCrYZ (Y = Ti, Zr, Hf and Z = Sn, Sb) exhibit a stable ferrimagnetic state, half metallic ferrimagnetism, 100% spin-polarization at the Fermi level and obeying to Slater-Pauling rule [15]. I. Galanak is confirms the linear comportment of the total spin magnetic moment as a function of number of valence electrons for two series of ordered quaternary Heusler alloys, which represent two variants of the Slater–Pauling rule [16]. The Slater-Pauling rules of magnetic materials relate their electronic properties (number of valence electrons in the unit cell) to their magnetic properties (total spin magnetic moment in the unit cell). The half-metallic nature of FeCrTiSi was mainly owing to the different behavior of the two spins. For spin-up state, FeCrTiSi carried a band gap of 0.809 eV [17]. Recent studies have highlighted the limitations of several conventional thermoelectric materials. For example, skutterudite-based compounds, although widely explored, rely heavily on filler atoms to suppress lattice thermal conductivity and improve ZT, which complicates synthesis and device reliability [18]. Similarly, XCoP (X = Ti, Zr, Hf) half-Heusler alloys exhibit semiconducting behavior with moderate bandgaps (1.29–1.40 eV) and ZT values in the range of 0.3–0.7 at 1200 K, which remain insufficient for high-efficiency energy conversion [19]. Another family of half-Heuslers, TiAgZ (Z = Al, Ga, In), has been reported as narrow band gap semiconductors (0.08–0.19 eV) with ZT values as low as 0.23–0.3 at 100 K, further restricting their practical applications [20]. In contrast, the MnNiSi half-Heusler alloy exhibits a stable cubic structure, semiconducting behavior with a bandgap of 0.57 eV, and ferrimagnetic properties. Its thermoelectric performance is remarkable, with a Seebeck coefficient of 118 μV/K and a high figure of merit (ZT = 1.52), making it a promising candidate for combined thermoelectric and spintronic applications [21]. Moreover, recent investigations on barium-based oxide perovskites $BaXO_3$ (X = Cr, Mn, Sc) revealed their structural stability in the ferrimagnetic phase and half-metallic behavior with integer spin magnetic moments, confirming their potential for spintronic applications. However, despite these interesting magnetic and thermodynamic properties, their thermoelectric efficiency has not been proven to reach competitive levels, particularly under operating conditions where thermal stability and reproducibility are critical [22]. This work consists of studying a new series of Fe-based FeCrTiM(M = Al, As, Si) quaternary Heusler alloys for data storage, energy conversion and optoelectronics applications. The ferrimagnetic case for the three types of quaternary Heusler is the most stable. These Heusler alloys are thermodynamically stable beyond 300 K because their negative Helmholtz free energy, which decreases with increasing temperature. This stability is more pronounced in FeCrTiAs. The no negative frequency phonon modes through the first Brillouin zone confirm their dynamic stability. The bands' structure indicates that the FeCrTiAl Heusler alloys is semiconductor in both spins, while FeCrTiSi and

Table 1 The values of $R_{MT}xK_{max}$, R_{MT} of each constituent and k-point for FeCrTiM (M = Al, As, Si) using GGA

	$R_{MT}xK_{max}$	R_{MT}(Fe)	R_{MT}(Cr)	R_{MT}(Ti)	R_{MT}(M)
FeCrTiAl	9.5	2.49	2.43	2.37	2.25
FeCrTiAs	9.5	2.44	2.38	2.32	2.32
FeCrTiSi	9.5	2.43	2.37	2.31	2.19

FeCrTiAs are spin-gapless semiconductors. The Heusler alloys family is a spin-gapless semiconductor material having a zero-band gap in the band structure of one spin channel but a finite band gap in the other spin channel.

2 Computational method

All calculations were performed using the WIEN2k package, which implements the full-potential linearized augmented plane-wave (FPLAPW) method [23]. The generalized gradient approximation (PBE-GGA) [24] of Perdew, Burke, and Ernzerhof, together with the modified Becke–Johnson exchange potential (mBJ-GGA) [25] within the projector augmented-wave framework, were employed for the optimization of the lattice constants as well as for the electronic, optical, and thermoelectric characterizations of FeCrTiM (M = Al, As, Si). The plane-wave cut-off parameter in the interstitial region (RMT × Kmax), the muffin-tin radii (RMT), the maximum plane-wave vector (Kmax), and the k-point meshes used in the irreducible Brillouin zone are summarized in Table 1. To ensure convergence and accuracy, 1500 k-points were used in the irreducible Brillouin zone for structural optimization, 5000 points for elastic properties, and 10000 points for optical and thermoelectric calculations. The energy convergence criterion was set to 10^{-5} Ry to achieve self-consistency, which guarantees reliable convergence of the total energy. It should also be noted that the Seebeck coefficient and the figure of merit (ZT) calculated separately for spin-up and spin-down channels differ from the combined values for the full material. The total Seebeck coefficient is calculated according to [26].

$$S = [S(\uparrow) \times \sigma(\uparrow) + S(\downarrow) \times \sigma(\uparrow)]/[\sigma(\uparrow) + \sigma(\downarrow)] \quad (1)$$

where S(↑) and S(↓) represent the Seebeck coefficients, and σ(↑) and σ(↓) the electrical conductivity for spin-up and spin-down states, respectively. Consequently, the total figure of merit ZT is computed based on this combined Seebeck coefficient, following the relation:

$$ZT = \left(S^2\sigma T\right)/\kappa \quad (2)$$

where.

$\kappa = \kappa_e(\uparrow) + \kappa_e(\downarrow) + k_L$ is the total thermal conductivity, $\kappa_e(\uparrow)$ and $\kappa_e(\downarrow)$ are the electronic thermal conductivities for spin-up and spin-down states respectively, and κ_l is the lattice thermal conductivity.There are several ways to determine the k_L of a substance. By using Slack's model [27] and Berman [28] demonstrated that the intrinsic k_L can be:

$$k_L = A\frac{\overline{M}\theta_D^3\delta}{\gamma^2 T n^{2/3}} \quad (3)$$

γ is the Grüneisen parameter, θ_D is the Debye temperature, and n is the number of atoms in the primitive unit cell. Also, $\overline{M}$ and δ^3 are the atoms' average mass in the crystal and the average volume occupied by one atom in the crystal, respectively. Julian [29] provides the following formula for calculating the parameter A.

$$A = \frac{2.43 * 10^{-8}}{1 - \frac{0.514}{\gamma} + \frac{0.288}{\gamma^2}} \quad (4)$$

Therefore, the total figure of merit when combining spin contributions can be written as:

$$ZT = \left([S(\uparrow) \times \sigma(\uparrow) + S(\downarrow) \times \sigma(\downarrow)]^2/(\sigma(\uparrow) + \sigma(\downarrow))\right) \times T/\left[\kappa_e(\uparrow) + \kappa_e(\downarrow) + k_L\right] \quad (5)$$

3 Results and discussions

3.1 Structural analysis

The quaternary Heusler alloys FeCrTiM (M = Al, As, Si) follow the general formula XX'YZ (1:1:1:1), where X, X', and Y represent rare earth or transition metals, and M belongs to elements from groups III, IV, and V. These alloys exhibit three distinct crystal structures type 1, type 2, and type 3 depending on the arrangement of their constituent atoms, as detailed in Table 2.

Table 2 Different structures for three types of quaternary Heusler compounds FeCrTiM (M = Al, As, Si) with Wyckoff positions

	4*a* (0,0,0)	4*c* (1/4,1/4,1/4)	4*b* (1/2,1/2,1/2)	4*d* (3/4,3/4,3/4)
type-I	M	Cr	Ti	Fe
type-II	M	Ti	Cr	Fe
type-III	Cr	M	Ti	Fe

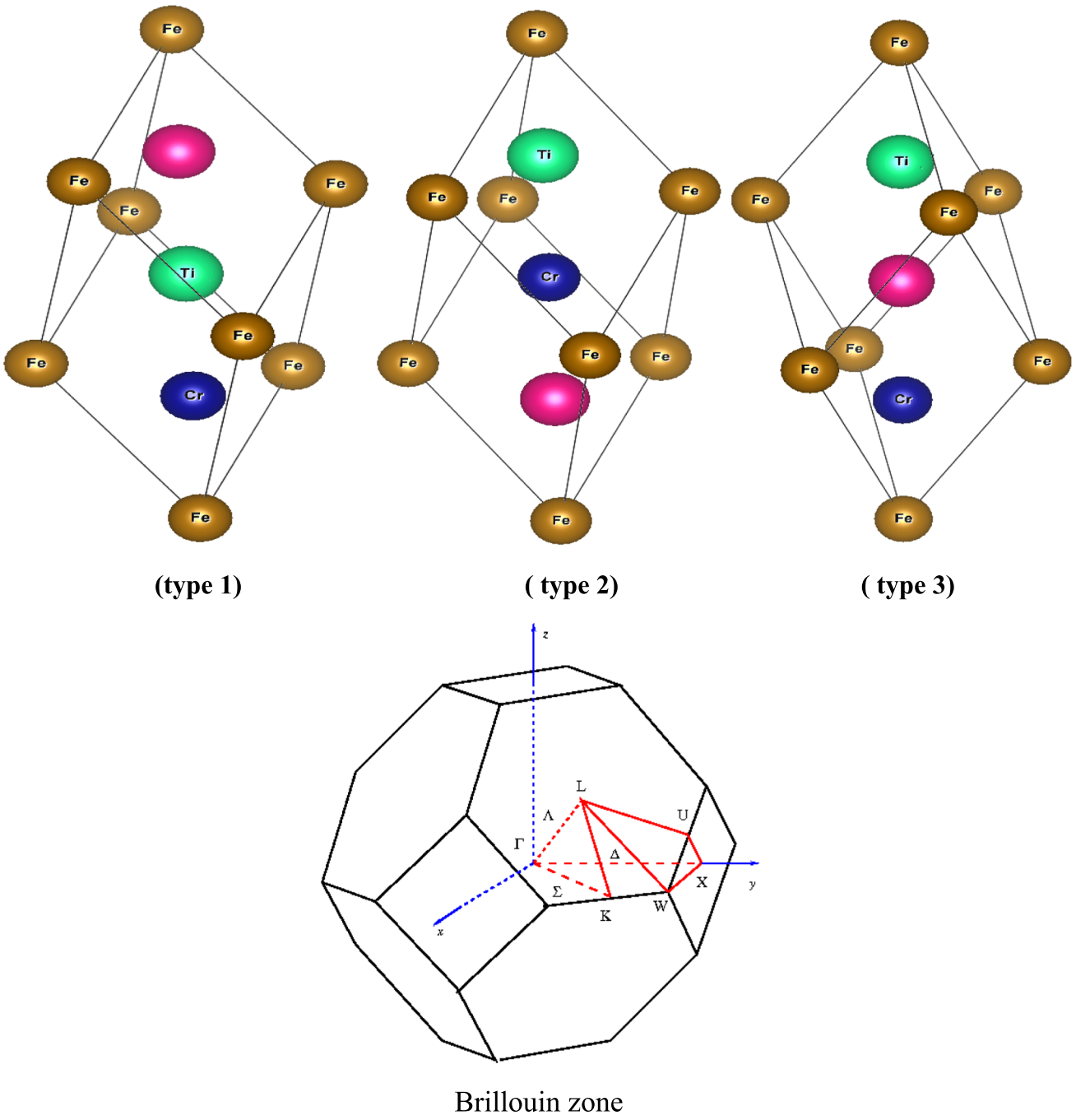

Fig. 1 Cubic crystal structure (atoms are colored as follows: Fe – brown, Cr – bleu, Ti– green, M– magenta) and the first Brillouin zone of the quaternary Heusler alloys FeCrTiM (M = Al, As, Si)

Table 3 Spin orientations of Fe, Cr, and Ti atoms in different magnetic configurations (FM, FIM1, FIM2, and NM) for quaternary Heusler FeCrTiM (M = Al, As, Si)

	Fe	Cr	Ti
FM	up(dn)	up(dn)	up(dn)
FIM1	up	Up	dn
FIM2	dn	Dn	up
NM	n	N	n

They adopt the LiMgPdSn-type crystal structure, with the primitive cell comprising four atoms, as illustrated in Fig. 1. Notably, the first Brillouin zone of the cubic structure, depicted in Fig. 1, plays a pivotal role in understanding the electronic and vibrational properties of these materials. The high-symmetry points within this zone are crucial for analyzing dispersion curves and electronic band structures, providing deep insights into the system's

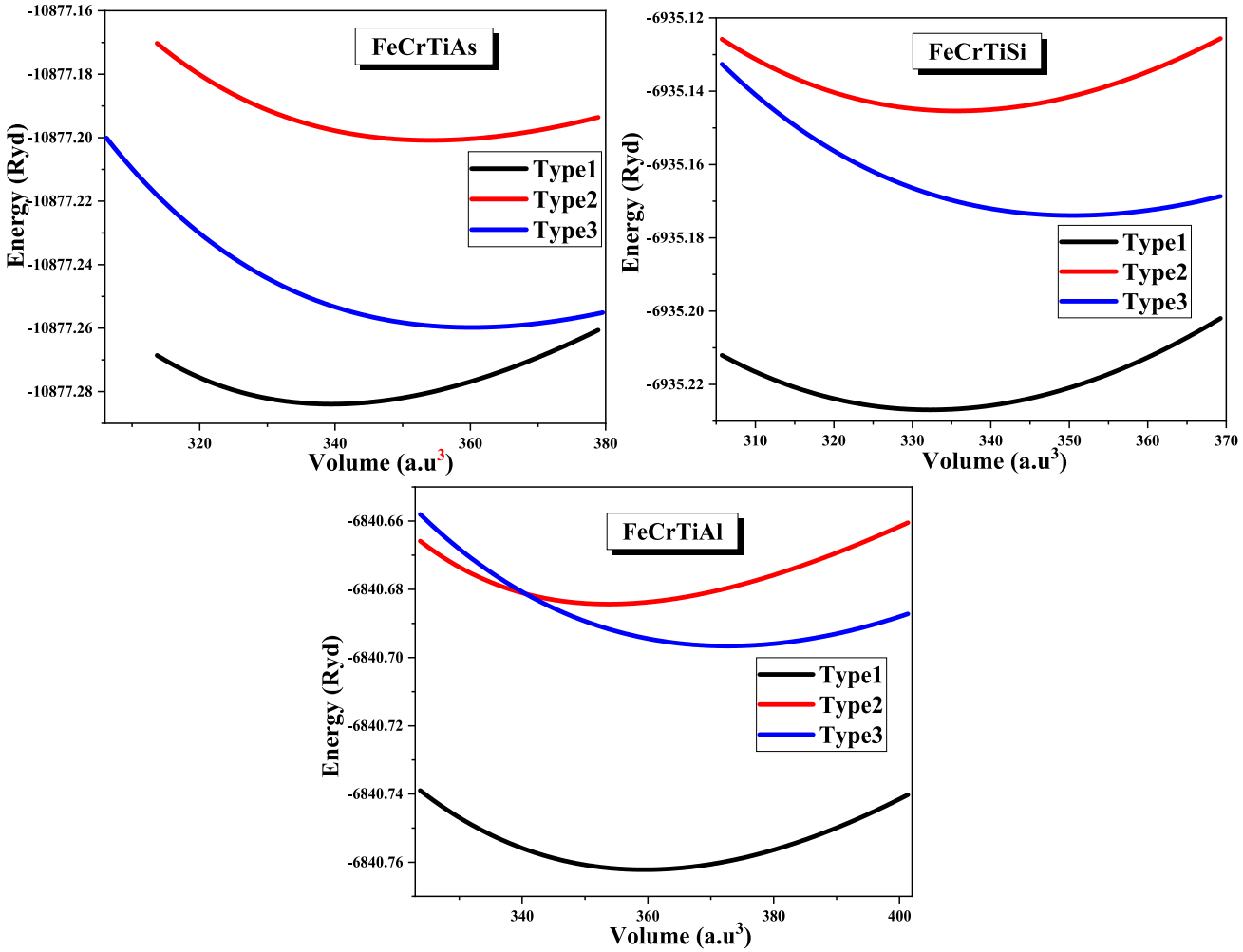

Fig. 2 Total energy as a function of volume in ferromagnetic case for the three types of quaternary Heusler FeCrTiM (M = Al, As, Si)

Table 4 Optimized lattice constants (a_0), bulk modulus (B), and its pressure derivative (B'), minimum total energy (E_0) and formation energy for quaternary Heusler alloys FeCrTiM (M = Al, As, Si)

		a_0 (Å)	B (GPa)	B'	E_0 (Ry)	ΔH_f (eV/atom)
FeCrTiAl	type 1	5.972	160.395	4.296	−6840.762157	−1.63
	type 2	5.941	161.398	8.062	−6840.684337	
	type 3	6.044	140.941	3.951	−6840.696615	
FeCrTiAs	type 1	5.859	192.409	5.850	−10877.283940	−1.05
	type 2	5.942	144.130	6.593	−10877.200811	
	type 3	5.976	146.160	6.402	−10877.259752	
FeCrTiSi	type 1	5.817 5.821[17]	194.382 219.041[17]	1.367 2.902[17]	−6935.226900	−0.774
	type 2	5.837 5.836[17]	193.647 211.331[17]	2.653 3.455[17]	−6935.145382	
	type 3	5.922 5.917[17]	166.383 186.656[17]	4.424 3.705[17]	−6935.173883	

behavior. The atomic configuration of the crystal has a considerable effect on the physical properties of alloys. Therefore, we determine the total energies for the different atomic arrangements (1, 2, 3) in order to specify the most stable structure for the ferrimagnetic state (Table 3).

Figure 2; shows the energy as a function of volume in ferrimagnetic case for the three types of quaternary

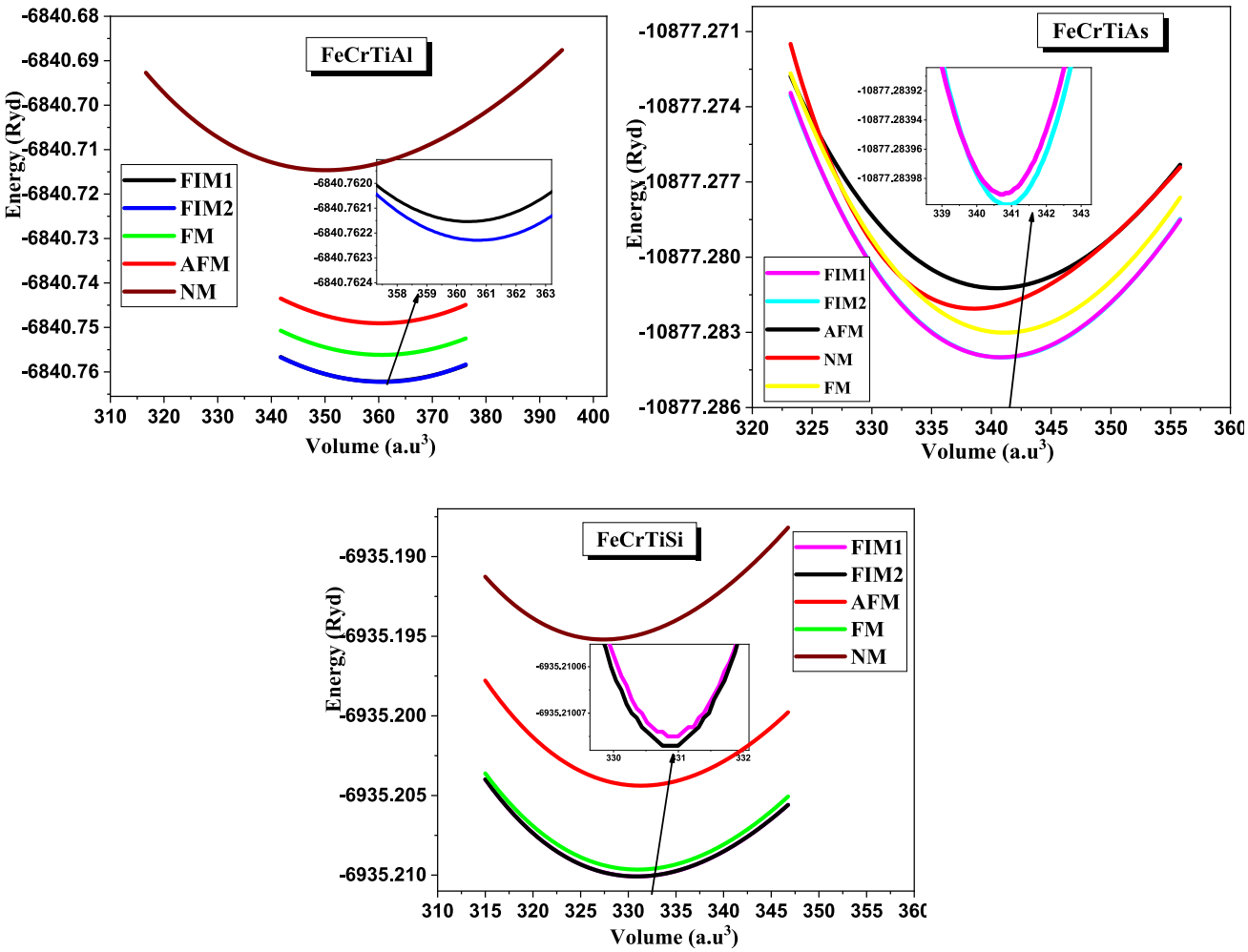

Fig. 3 Total energy as functions of unit cell volume in nonmagnetic, ferromagnetic, ferrimagnetic, and antiferromagnetic states in type 1-structure for quaternary Heusler alloys FeCrTiM (M = Al, As, Si)

Heusler compounds FeCrTiM(M = Al, As, Si). The negative formation energy values (Table 4) imply that all the studied Heusler compounds are energetically stable and could be synthesized experimentally under ambient conditions, in agreement with previous theoretical predictions on similar systems [30, 31]. The theoretical formation energy predicts that the 1 state is more stable than those of types 3 and 2. It is important to note that this structural stability refers to the atomic arrangement (type-1 vs. type-2 vs. type-3), while the following section discusses the relative stability of the different magnetic configurations.

We present in Fig. 3 shows the structural optimization curves in the ferromagnetic (FM), ferrimagnetic (FIM1, FIM2), antiferromagnetic (AFM), and nonmagnetic (NM) phases, fitted to the Murnaghan equation of state [32]. The corresponding spin orientations of Fe, Cr, and Ti atoms in each magnetic configuration are summarized in Table 3, where it is evident that the ferrimagnetic states (FIM1 and FIM2) exhibit antiparallel alignment of Ti relative to Fe and Cr, in contrast to the fully parallel spin alignment in the FM case. From the energy–volume curves, it is clear that the ferrimagnetic (FIM) phase is more stable than FM, AFM, and NM states, confirming that the ground state of the studied Heusler alloys is ferrimagnetic. The relative stability follows the order: FeCrTiAs > FeCrTiSi > FeCrTiAl.

The equilibrium lattice constants obtained in the quaternary Heusler alloys under study, together with their ground-state energies, bulk modulus, and its derivative with respect to pressure calculated using the Birch–Murnaghan equation of state, are summarized in Table 4. The equilibrium lattice constant of FeCrTiSi is in good agreement with previous results using GGA-PBE and LSDA functionals within the WIEN2k code [17]. To the best of our knowledge, no optimized lattice constants and ground-state parameters were previously reported for FeCrTiAs and FeCrTiAl, hence our

results provide theoretical predictions in agreement with similar Heusler systems [30–32]. Recent theoretical studies on half-Heusler alloys have highlighted their multifunctional potential in spintronics and thermoelectrics. For instance, TaMnZ (Z = As, Sb, Bi) compounds were found to be stable in the ferrimagnetic cubic phase, showing half-metallic behavior with indirect band gaps, full spin polarization, integer magnetic moments, and favorable thermoelectric figures of merit [33]. Similarly, other cubic half-Heusler alloys have been reported to stabilize in the ferrimagnetic phase, exhibiting half-metallic character with indirect or direct band gaps in the spin-up channel, integer magnetic moments, and promising transport properties that support their spintronic and thermoelectric applications [34]. In addition, alkali-based LiCrZ (Z = Ge, Sn, Pb) systems were shown to undergo a transition from a stable ferrimagnetic to a more stable antiferromagnetic phase, consistent with the Slater–Pauling rule, while maintaining half-metallic nature, high Curie temperatures, and excellent thermoelectric performance [35]. These results are consistent with our present findings on FeCrTiM compounds, further confirming their stability and half-metallicity, and underlining their potential in multifunctional device applications. Figure 3; the structural optimization curves in the ferrimagnetic and nonmagnetic phases fitted to the Murnaghan equation of state [32]. Then we determine the properties of the ground state such as the lattice constant, the bulk modulus, as well as its derivative with respect to the pressure and the minimum formation energy. All Heusler under study in the ferrimagnetic phase have lower energies than the nonmagnetic one. Therefore, the ferrimagnetic phase is the most stable than the nonmagnetic state. The stability of FeCrTiAs is better than those of FeCrTiSi and FeCrTiAl respectively. The equilibrium lattice constant obtained in the quaternary Heusler alloys under study with their ground state energies, the bulk modulus and its derivative with respect to the pressure obtained using the Birch–Murnaghan equations of state are presented in Table 4. The equilibrium lattice constant of FeCrTiSi for all types structures is in good agreement with the reported values calculated using the GGA-PBE and LSDA functional as executed in the WIEN2k code [17]. No studies on optimized lattice constants and other ground state parameters have been performed on FeCrTiAs and FeCrTiAl compounds, hence our results are predictions. Figure 4 shows the Helmholtz free energy as a function of temperature for FeCrTiSi, FeCrTiAs, and FeCrTiAl quaternary Heusler alloys in the harmonic approximation, where these compounds are thermodynamically stable above room temperature because of their negative Helmholtz free energy and its decrease with increasing temperature. The thermodynamic stability of FeCrTiSi is better than those of FeCrTiAl and FeCrTiAs respectively. It can be obviously seen that there are no.

imaginary phonon frequencies in the entire Brillouin zone as shown in Fig. 5, which proves that these considered crystals are dynamically stable under environmental pressure. The optical mode for frequencies located beyond 8 cm^{-1} for FeCrTiAl, FeCrTiAs, and FeCrTiSi is mainly due to the vibrations of Al, Cr, and Si atoms, and two atoms

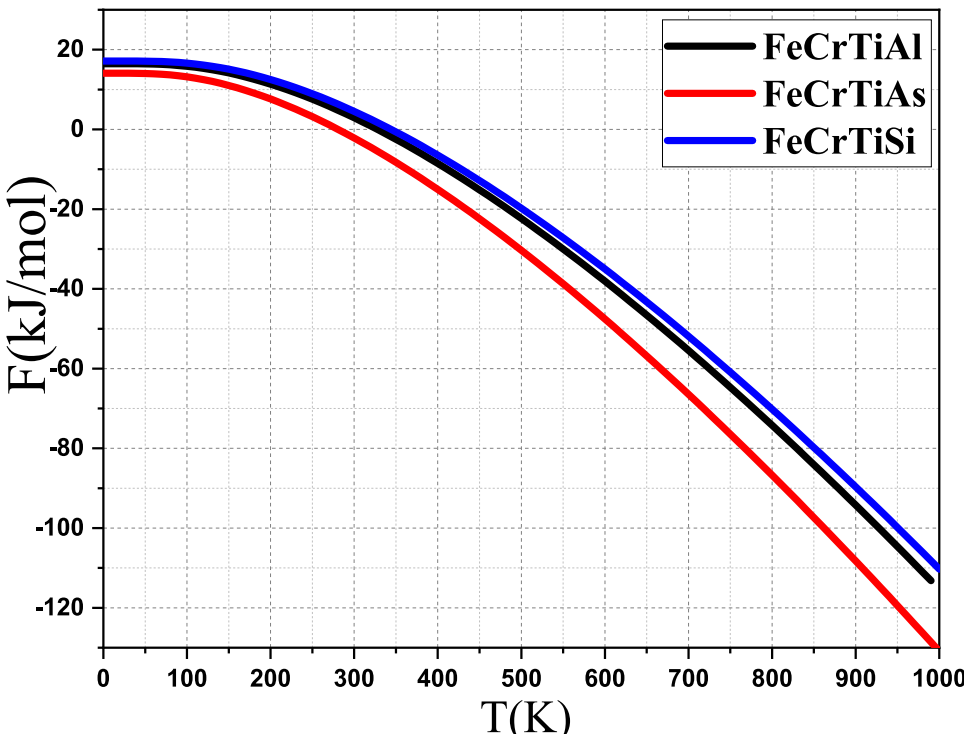

Fig. 4 Helmholtz free energy as function of temperature for FeCrTiAl, FeCrTiAs, and FeCrTiSi compounds in the harmonic approximation

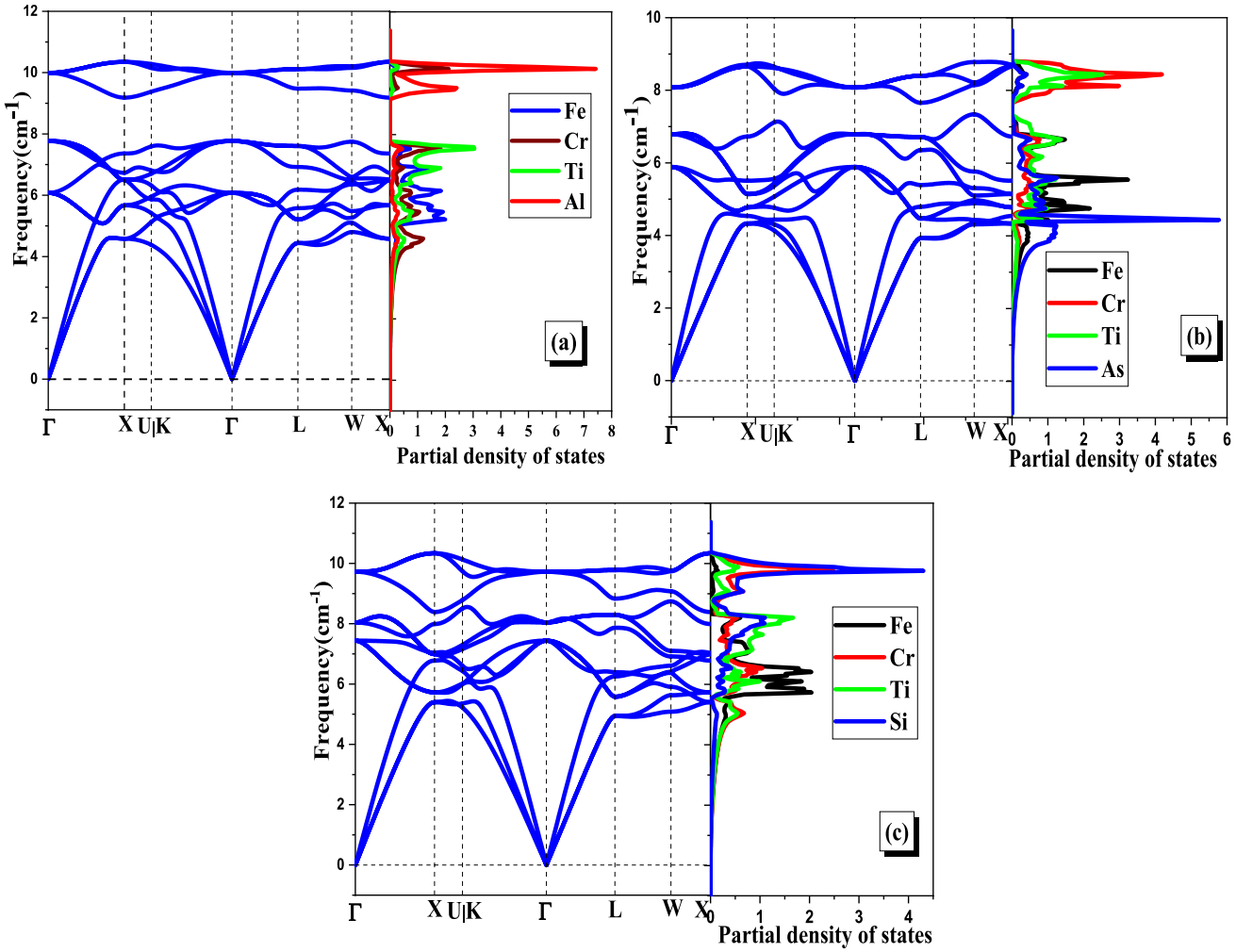

Fig. 5 Phonon dispersions curves and projected density of states for FeCrTiAl (a), FeCrTiAs (b) and FeCrTiSi (c) computed by Phonopy with GGA approaches

in the unit cell vibrate in an opposite direction. While, the acoustic mode with frequencies below 8 cm^{-1} is governed by the vibrations of the Fe and Ti atoms in the same direction. It should be emphasized that this Helmholtz free energy analysis reflects the thermodynamic stability as a function of temperature, whereas the subsequent phonon dispersion results (Fig. 5) demonstrate the dynamic stability, i.e., the absence of imaginary vibrational modes.

3.2 Elastic constants and related mechanical parameters

The quaternary Heusler alloys FeCrTiM (M = Al, As, Si) so-called LiMgPdSn Y-type cubic structure with F-43m (2 1 6) space group. The mechanical analysis of these materials is determined using elastic moduli C_{11}, C_{12}, C_{44} and B with finite strain theory as reported in Table 5.

For cubic crystals, the Born stability criteria require that the independent elastic constants satisfy the following conditions [36]:

$$0\langle C_{11}, 0\langle C_{44}, 0\langle C_{11} - C_{12}, 0\langle C_{11} + 2C_{12}, C_{12}\langle B\langle C_{11}\rangle \quad (6)$$

These conditions have been verified, which ensures the mechanical stability of all the studied compounds.

For cubic crystal, the module of the compressibility $B$is given by the following expression: $B = (C_{11} + +2C_{12})/3$ [37], while the shear modulus G was obtained using the Voigt-Reuss-Hill (VRH) method [38–41], the shear modulus G is given by the following expression:

$$G = \frac{G_R + G_R}{2} \quad (7)$$

where, G_R is given by:

Table 5 Elastic constants (C_{11}, C_{12}, C_{44}), shear modulus (G_V, G_R, G_H), bulk modulus (B_V, B_R, B_H), anisotropy factor (A), Young's modulus (E_V, E_R, E_H), Poisson's coefficient (ν_V, ν_R, ν_H) and Pugh's criterion B_H/G_H ratio for FeCrTiM (M = Al, As, Si) Heusler compounds

	FeCrTiAl	FeCrTiAs	FeCrTiSi
C_{11} (GPa)	263 264.2 [8]	275.7	288 271 [8]
C_{12} (GPa)	112.7 109 [8]	143.4	181.3 168
C_{44} (GPa)	112.2 107.3 [8]	64.8	106 114.2 [8]
G_v (GPa)	97.4	65.3	84.9
G_R (GPa)	93.7	65.3	76
G_H (GPa)	95.6	65.3	80.4
B_H (GPa)	162.8 160.6 [8]	187.5	216.8 202.3 [8]
A	1.49 1.38 [8]	0.98	1.98 1.95 [8]
E_V (GPa)	243.7	175.7	225.4
E_R (GPa)	236	175.7	204.1
E_H (GPa)	239.8	175.7	214.8
ν_v	0.25	0.34	0.32
ν_R	0.25	0.34	0.34
ν_H	0.25	0.34	0.33
Pugh's criterion (B_H/G_H)	1.7	2.86	2.69

$$G_R = \frac{5(C_{11} - C_{12})C_{44}}{4C_{44} + 3(C_{11} - C_{12})} \tag{8}$$

while G_V is defined as:

$$G_V = \frac{(3C_{44} + C_{11} - C_{12})}{5} \tag{9}$$

The Young modulus E and the Poisson's ratio ν are calculated respectively, using the following expressions [37]:

$$E = 9BG/(3B + G) and v = (3B - 2G)/(6B + 2G) \tag{10}$$

The anisotropy factor A, which measures the degree of elastic anisotropy in cubic crystals, is defined as [37].

$$A = \frac{2C_{44}}{C_{11} - C_{12}} \tag{11}$$

We report in Table 5 the shear and bulk moduli, universal anisotropy factor, Young's moduli, Poisson's ratio and Pugh's criterion of isotropic polycrystalline materials using the Voigt-Reuss-Hill approximation. Fairly large elastic constants reflect large inter-reticular distances, bond strength and average hardness. The average values of bulk modulus, shear and Young's moduli confirm their average hardness and rigidity. Poisson's ratio is dimensionless and ranges between 0.1 and 0.45. Low Poisson's ratio, such as 0.1–0.25, means rocks fracture easier whereas high Poisson's ratio, such as 0.32–0.45, indicates the rocks are harder to fracture. The positive Poisson's ratio of these materials indicates no deformation of microstructures. According to the calculated Poisson's ratio values (Table 4), FeCrTiAs ($\nu = 0.34$) and FeCrTiSi ($\nu = 0.33$) exhibit metallic bonding characteristics ($\nu \geq 0.33$), whereas FeCrTiAl ($\nu = 0.25$) suggests predominantly covalent bonding nature. The three-dimensional graphs of Young's modulus and their transverse sections in separated planes are illustrated in Fig. 6. This parameter reported to be anisotropic inFeCrTiAl and FeCrTiSi, while it is isotropic for FeCrTiAs. The universal anisotropy factor reported in Table 5 confirms the previous result. According to Pugh's criterion**,** a B/G ratio greater than 1.75 typically indicates ductile behavior, whereas a ratio below 1.75 indicates brittleness. According to Pugh's criterion (B/G), FeCrTiAl (B/G = 1.70) exhibits brittle behavior, whereas FeCrTiAs (B/G = 2.86) and FeCrTiSi (B/G = 2.69) exhibit ductile behavior. This observation is consistent with previous reports on quaternary Heusler alloys [42].

3.2.1 Debye temperature and Grüneisen parameter

To further elucidate the lattice dynamics, we estimated the Debye temperature Θ_D from the average sound velocity v_m , obtained using the Voigt–Reuss–Hill elastic moduli and the mass density ρ. The transverse and longitudinal sound velocities are:

$$v_l = \left(\frac{3B + 4G}{3\rho}\right)^{1/2} and v_t = \left(\frac{G}{\rho}\right)^{1/2} \tag{12}$$

and the average sound velocity is:

$$v_m = \left[\frac{1}{3}\left(\frac{2}{v_t{}^3} + \frac{1}{v_l{}^3}\right)\right]^{-1/3} \tag{13}$$

The Debye temperature is then given by:

$$\theta_D = \frac{h}{k_B}\left(\frac{3}{4\pi V_a}\right)^{1/3} v_m \tag{14}$$

where h is Planck's constant, k_B is Boltzmann's constant, N_A is Avogadro's number, and M is the molar mass per formula unit. In the absence of full quasi-harmonic data, we estimated the Grüneisen parameter using an isotropic Anderson-type relation that links γ to Poisson's ratio.

$$\gamma = \frac{3}{2} \times \frac{\upsilon + 1}{3\upsilon - 2} \tag{15}$$

The Debye temperature ΘD was calculated according to Eqs. (12–14). The Grüneisen parameter γwas evaluated using the isotropic Anderson-type relation (Eq. 15). The calculated results are summarized in Table 6. The highest

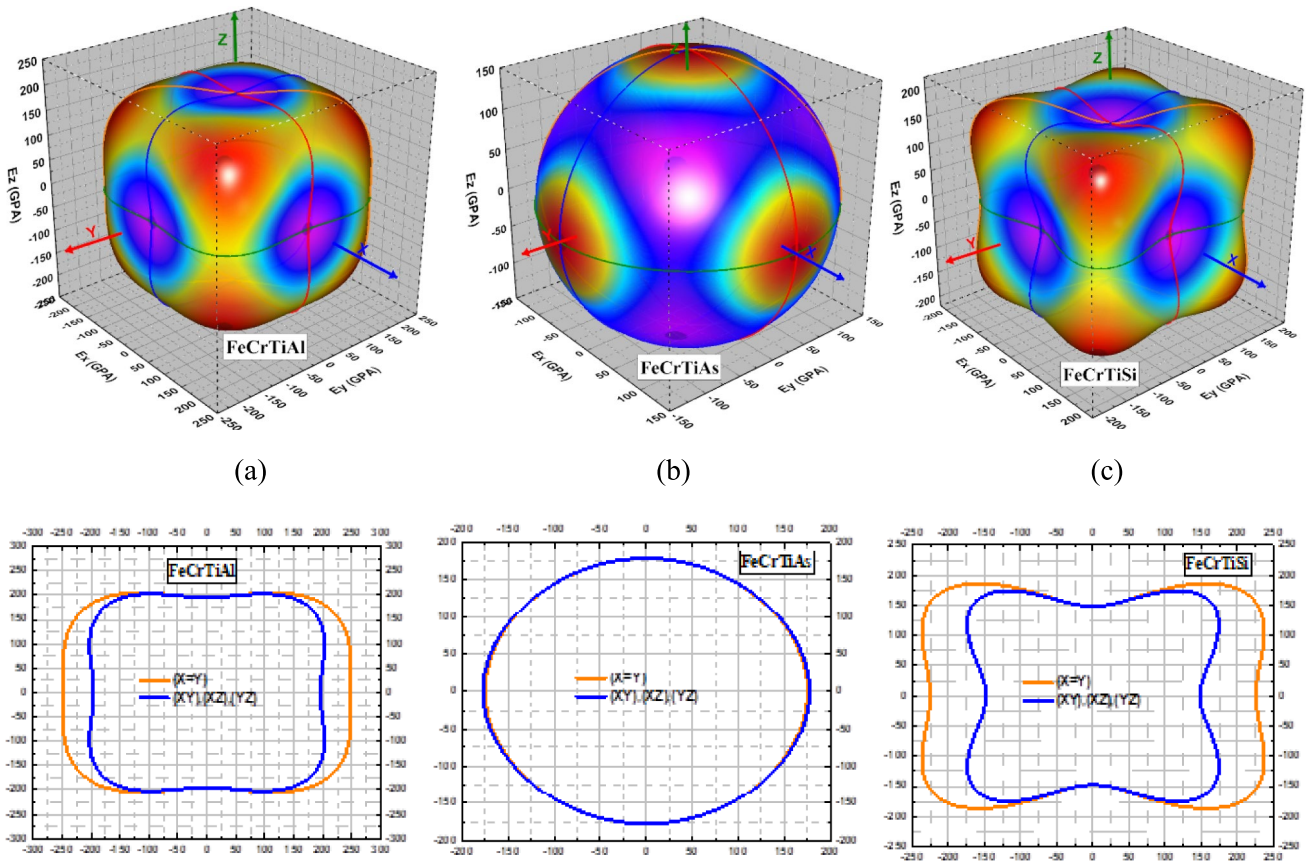

Fig. 6 Graphs of the 3D surface of the Young's modulus **a** FeCrTiAl, **b** FeCrTiAs, **c** FeCrTiSi, **d** and **e** and **f**, their transverse sections in separated planes, respectively

Table 6 Calculated transverse (*Vt*), longitudinal (*Vl*), and average (*Va*) sound velocities, Debye temperature (ΘD), and Grüneisen parameter (γ) for FeCrTiM (M = Al, As, Si) quaternary Heusler alloys

	FeCrTiAl	FeCrTiAs	FeCrTiSi
Transverse elastic wave velocity V_t(m/s)	4094.365	2930.709	3595.775
Longitudinal elastic wave velocity V_l(m/s)	7134.506	6006.932	7216.778
The average wave velocity V_a(m/s)	4547.908	3292.295	4034.618
Debye Temperature(K)	571.509	421.490	520.969
γ	1.50	2.05	1.98

Debye temperature was obtained for FeCrTiAl, indicating stronger average interatomic bonding and lattice stiffness, in agreement with its large elastic constants. FeCrTiAs exhibits the lowest ΘD, reflecting softer lattice vibrations. The Grüneisen parameters for FeCrTiAs and FeCrTiSi are larger, implying stronger lattice anharmonicity, which favors reduced lattice thermal conductivity and enhanced thermoelectric performanceconsistent with the observed ZT≈1 and temperature-dependent trends of κ_L.

3.3 Spin-gapless semiconductors

Spin-gapless semiconductors are a distinct class of materials characterized by novel spin-dependent electronic properties arising from their unique electronic structure. Their band structure exhibits an energy gap for one particular spin orientation. The electronic and magnetic properties of a ferrimagnetic semiconductor are sensitive to spin state configurations, because energy differences are adopted in electronic transitions between orbits. Using first-principles density functional calculations, electronic band structure and density of states are needed to be inspected in spin-up and spin-down cases using GGA and mBJ-GGA approximations

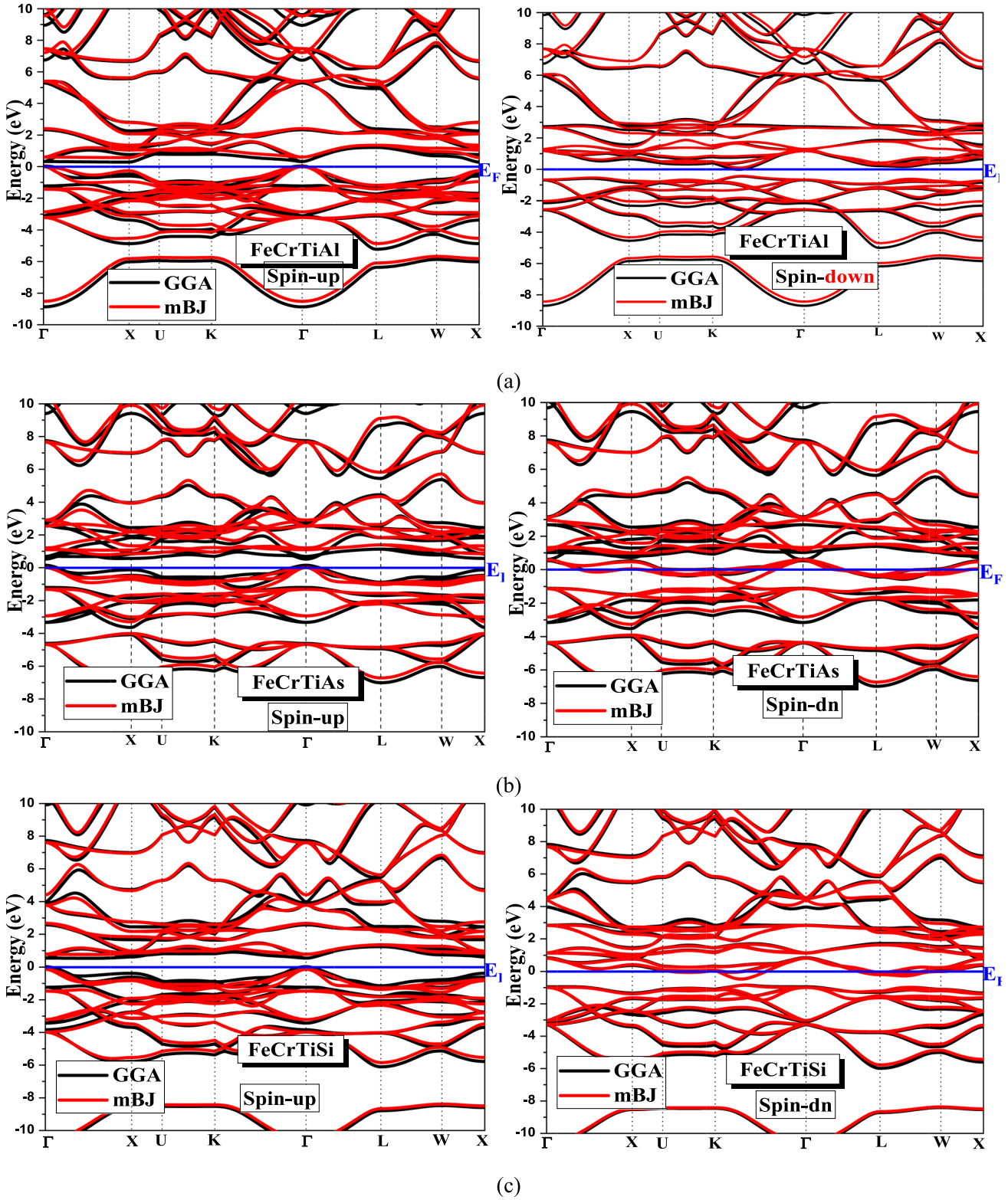

Fig. 7 Spin-up (left panel) and spin-down (right panel) band structure of FeCrTiAl **a**, FeCrTiAs **b** and FeCrTiSi **c** using GGA and mBJ-GGA approximations

in the ferrimagnetic phase along high-symmetry points of the first Brillouin zone. Figure 7 shows spin-up (left panel) and spin-down (right panel) band structure of FeCrTiAl (a), FeCrTiAs (b) and FeCrTiSi (c). For the spin-up, all Heuslers under study have a direct Γ-Γ band gap. For the spin-dn, FeCrTiAl is indirect Γ-L band gap semiconductor, while FeCrTiAs and FeCrTiSi are metallic. Based on the band structure calculations with GGA and mBJ-GGA, we have identified that FeCrTiAs and FeCrTiSi are spin-gapless semiconductors. The spin-gapless semiconducting and half-metallic behaviors observed in FeCrTiSi and FeCrTiAs are consistent with earlier findings on Fe- and Mn-based quaternary Heusler alloys [43, 44]. For FeCrTiAs, a very small overlap is observed in the spin-up channel, as shown in Fig. 7(b). However, this overlap is negligible and does not close the band gap completely. Therefore, the compound retains nearly 100% spin polarization at the Fermi level, confirming its half-metallic ferrimagnetic character.

For the spin-down, FeCrTiAl is indirect band gap semiconductor. For comparison, in spin-up, FeCrTiSi carried a direct band gap of 0.809 eV, whereas FeCrTiGe carried an indirect band gap of 0.629 eV [17]. We report in Table 7 the electronic state of FeCrTiM (M = Al, As, Si) using GGA and mBJ-GGA within spin-up and spin-down. FeCrTiAl belongs to the SGS family because it has a larger energy gap in the case of spin-down, while the Fermi level is located in a zero-energy gap in the spin-up band structure. FeCrTiSi is reported to be almost SGS, because in the spin-down electronic band structure there is a small overlap of bands above and below the Fermi level between the Γ and L points of the zone by Brillouin. In Fig. 8, we have gathered the Calculated elements and spin resolved density of states PDOS and TDOS of FeCrTiAl (a), FeCrTiAs (b) and FeCrTiSi (c) at equilibrium for an energy window around the Fermi level. Positive and negative PDOS indicate majority and minority spin contributions, correspondingly. The top edge of the valence band is derived primarily from Fe and Cr orbits for both spin-up and spin-dn in all quaternary Heusler alloys under study. We observe a hybridization of the Fe, Cr and Ti states at the top of the valence band for the two spin states and for all compounds under study. For the spin-up, FeCrTiSi and FeCrTiAs materials are semiconductors in both. The quaternary Heusler under study obey to the Slater-Pauling rule, where its origin can be explained in terms of orbitals hybridization. Whereas, in spin-down case, they show the metallic character for both approaches. FeCrTiAl is semiconducting material for both spin and both approaches.

Table 7 Band gap of FeCrTiM (M = Al, As, Si) using GGA and mBJ-GGA within spin-up and spin-down

	GGA		mBJ-GGA	
	spin-up	spin-down	spin-up	spin-down
FeCrTiAl	0.279	0.759	0.68	0.77
FeCrTiAs	0.375	Metal	0.90	Metal
FeCrTiSi	0.52	Metal	0.760 0.809 [9]	metal

Figure 9; presents the partial density of states (PDOS) for FeCrTiZ (Z = Al, As, Si). In all compounds, the states near the Fermi level are mainly dominated by the Fe-d and Cr-d orbitals, indicating that the magnetic and transport properties are primarily governed by the transition-metal atoms. Ti shows minor contributions around E_F, while the main group element Z (Al, As, Si) contributes weakly with p states at energies away from E_F. These features confirm that the half-metallic/SGS character arises from the hybridization between Fe-d and Cr-d states, in agreement with the total DOS analysis.

Figure 10; represents the electronic densities of state sp, d, d-eg and d-t2g orbitals of Fe, Cr and Ti transition metal elements, s and p orbitals of Al with both spin using mBJ-GGA approach. Local octahedral coordination of Fe (3d), Cr (3d) and Ti (2d) atoms in FeCrTiAl for both spin gives two degenerate orbitals, such that d-eg and d-t2g. The valence band and the conduction band have mixed d-eg/d-t2g character. While Al atom participates by mostly 3p state. The t2g triplet dxy, dxz and dyz orbitals have lower energy, while eg doublet. The eg doublet dz^2 and $d(x^2-y^2)$ orbitals have higher energy. These split d-orbitals are called t2g and eg because they are split by the effect of the surrounding ligand ions. The octahedral splitting energy is the energy difference between the t2g and eg orbitals. The effect of the crystal field increases the energy of the t2g orbitals, which point towards neighboring Al atoms. In the case of FeCrTiSi, there is a gap in both spin directions but the two gaps are not located at the same energy region and the Fermi level touches the right edge of the spin-down gap. The anti-bonding states (Fe, Cr, Ti)—(Si, Al, As) and no zero PDOS near the Fermi level for both spins reduce the energy of the occupied states eg, which have lower energy than the t2g, this explains the metallic character of the Heusler alloys studied. As a result, these states have lower energy than the t2g states in the valence band of Heusler alloys under study. The energy difference between the bottom of the t2g and eg states is consistent with an increasing degree of anti-bonding (Fe-Si, Cr-Si, Ti-Si). The total density of states at the Fermi level, $N(E_F)$, is obtained directly from the spin-resolved DOS by integrating the contributions of the spin-up and spin-down channels at E_F. Specifically, $N_{\uparrow}(E_F)$ and $N_{\downarrow}(E_F)$ are read from the calculated DOS curves at the Fermi energy. The spin polarization P is then calculated using the standard relation:

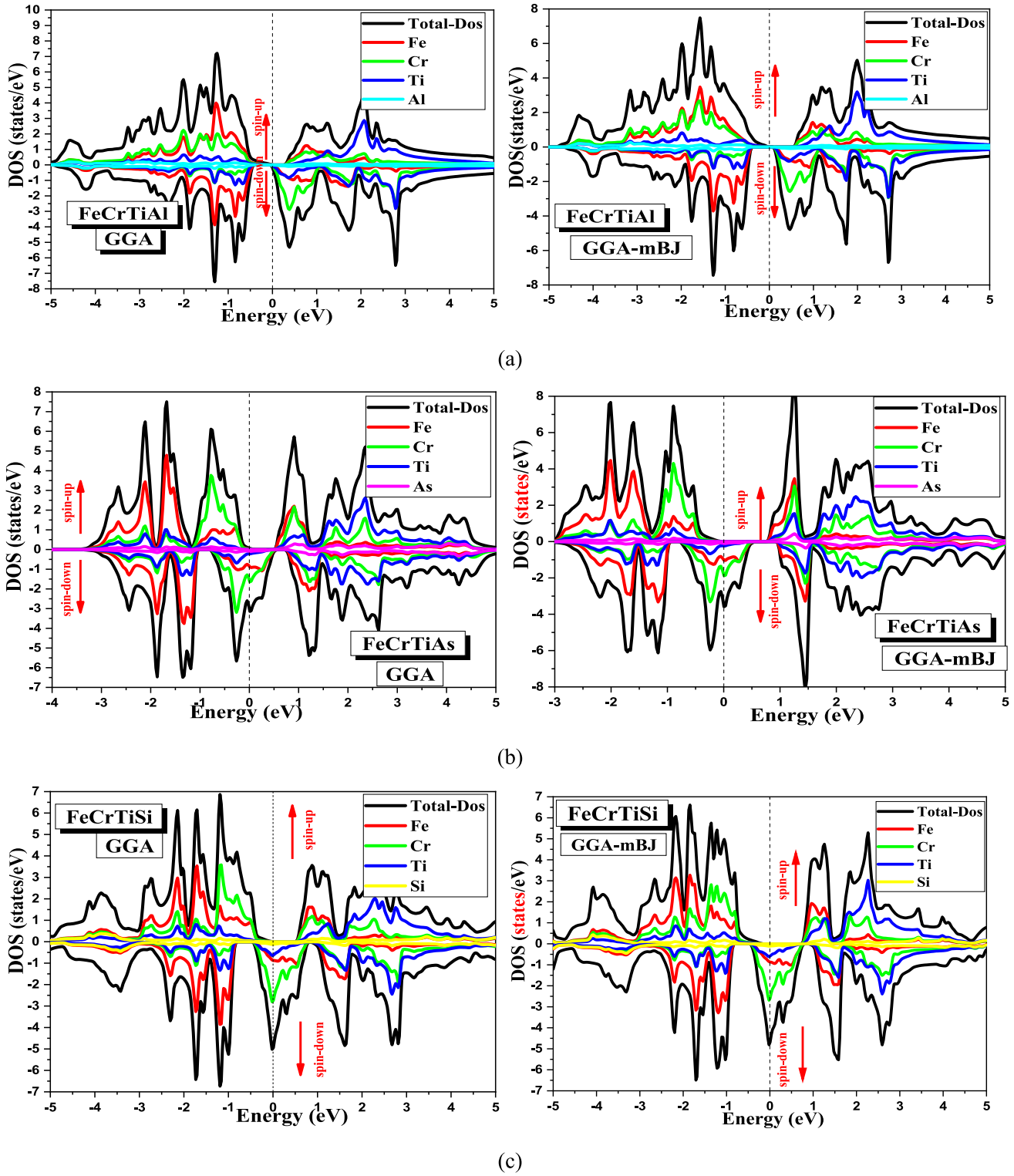

Fig. 8 Density of states (spin-up and spin-down) using GGA and mBJ-GGA approximations for **a** FeCrTiAl, **b** FeCrTiAs, and **c** FeCrTiSi compounds

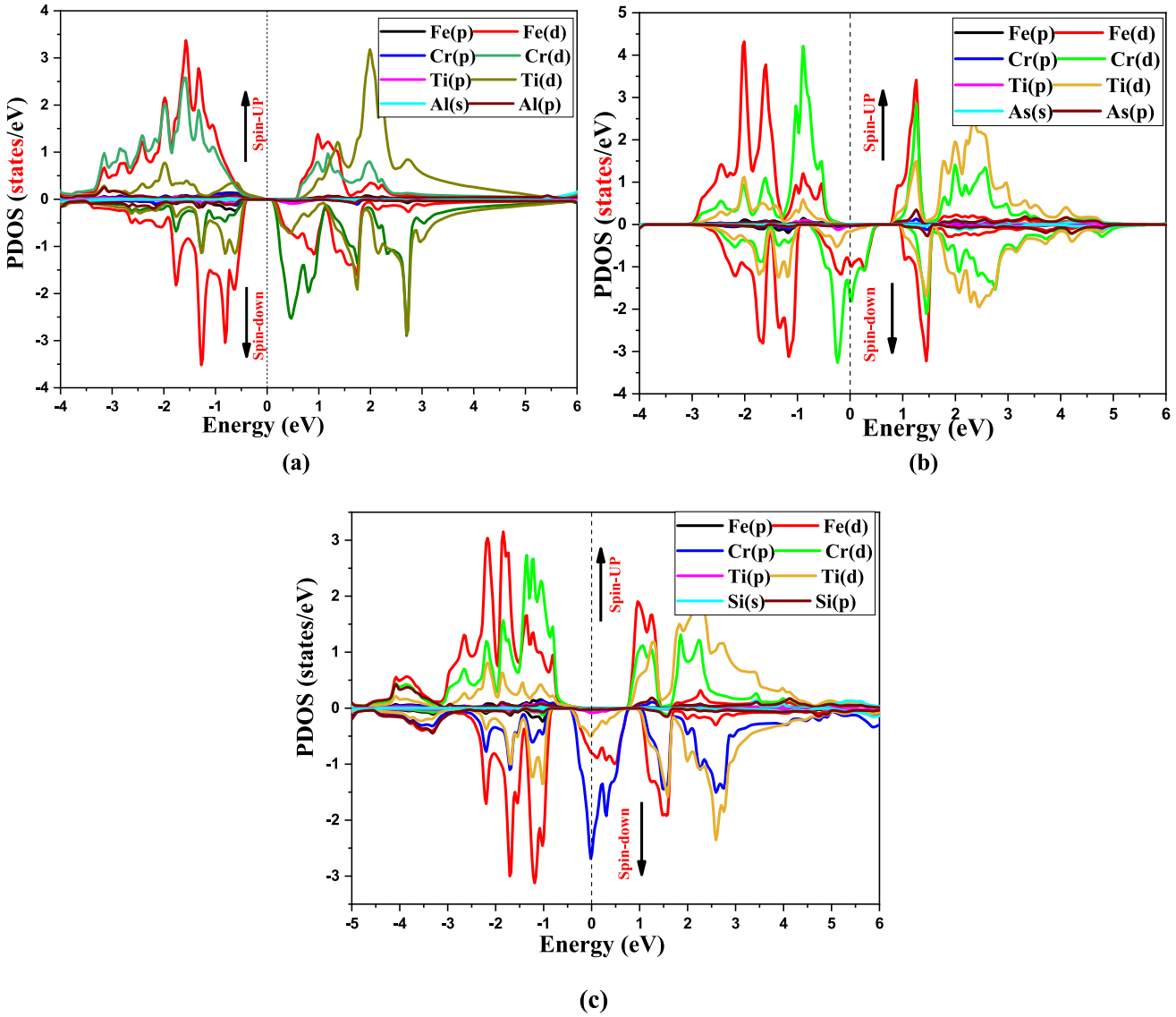

Fig. 9 Partial density of states for **a** FeCrTiAl **b** FeCrTiAs and **c** FeCrTiSi

$$P = \frac{N_{\downarrow}(E_F) - N_{\uparrow}(E_F)}{N_{\downarrow}(E_F) + N_{\uparrow}(E_F)} \times 100 \tag{16}$$

For half-metallic systems, $N_{\downarrow}(E_F)$, depending (or $N_{\uparrow}(E_F)$, depending on the spin channel) vanishes, which yields nearly P≈100%. In the present work, the values of $N(E_F)$ for both spin channels were extracted from our DOS calculations, and the resulting polarization was confirmed to approach full spin polarization at the Fermi level.

The Total Electron Density $N(E_F)$ up and down at Fermi level with P polarization for Heusler Quaternary Compounds FeCrTiZ (Z = Al, As, Si) calculated using both GGA and mBJ-GGA approximations, are presented in Table 8.

3.4 Magnetic properties

We have performed the spin polarized DFT calculations with GGA and mBJ-GGA approximations in the study of magnetic properties for FeCrTiAl, FeCrTiAs and FeCrTiSi Heusler alloys. The DOS and PDOS for up and down spin d-electrons using GGA and mBJ-GGA are shown in the Fig. 8. The magnetic moment of the atoms constituting the Heusler listed in Table 9, the interstitial and total magnetic moments for FeCrTiM (M = Al, As, Si), using GGA and mBJ-GGA approximations. These values are moderate rather than very high, yet they follow the linear trend predicted by the Slater–Pauling rule, confirming the half-metallic character of the studied Heusler alloys. These compounds exhibit ferrimagnetic character with major contribution to

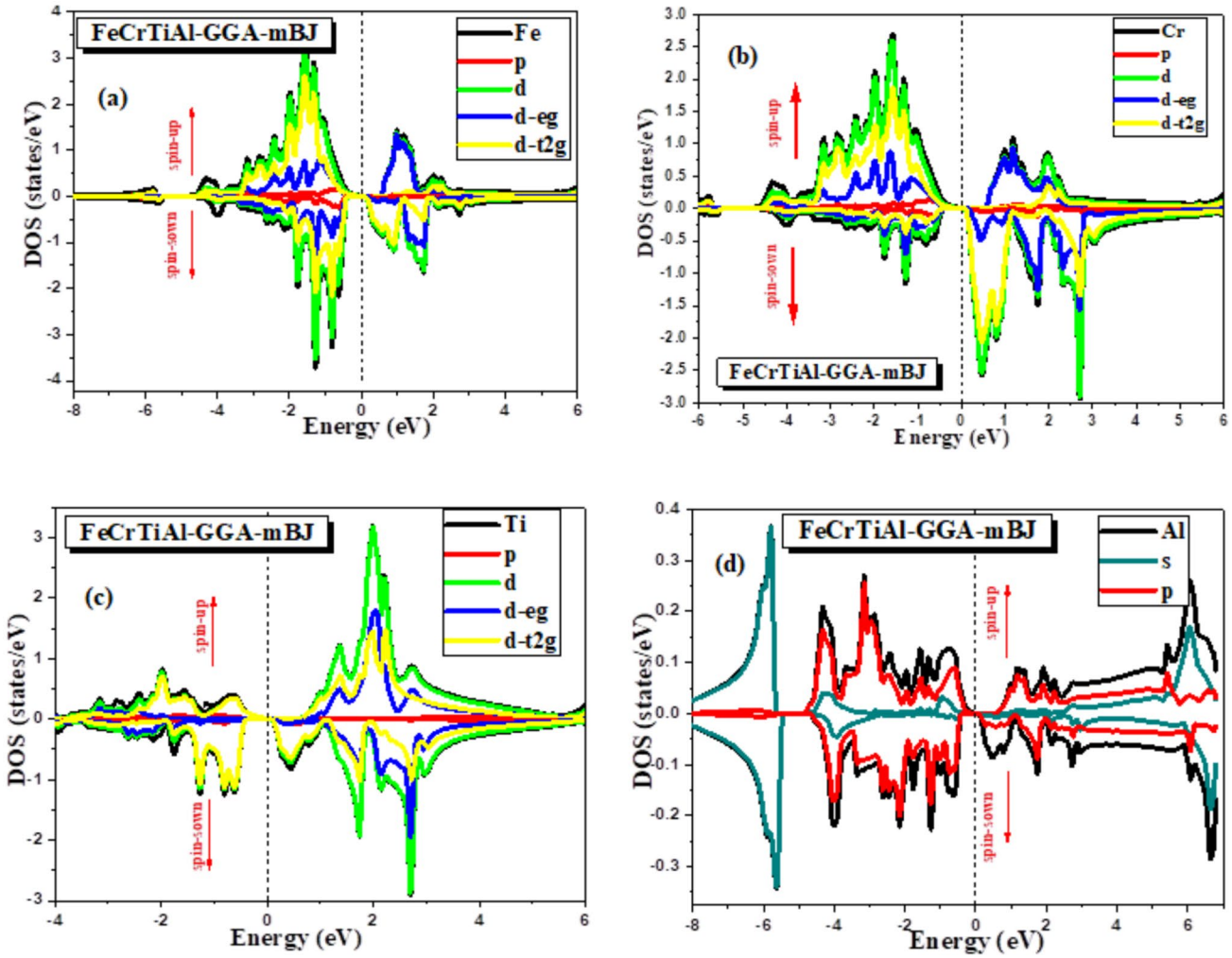

Fig. 10 Partial state density of FeCrTiAl for atoms **a** Fe, **b** Cr, **c** Ti, **d** Al calculated using GGA-mBJ

Table 8 Total electron density $N(E_F)$ up and down at Fermi level with *P* polarization for Heusler Quaternary Compounds FeCrTiM (M = Al, As, Si) calculated by GGA and mBJ-GGA approximations

	GGA			*GGA-mBJ*		
	$N(E_F)$ up	$N(E_F)$ down	*P*	$N(E_F)$ up	$N(E_F)$ down	*P*
FeCrTiAl	0.10	1.35	86.2%	0	0	0%
FeCrTiAs	0.91	45.09	96%	0.01	50.36	99.96%
FeCrTiSi	0.03	70.57	99.91%	0.00	66.87	100%

the magnetization comes from the unfilled Fe-3d and Cr-3dorbitals.We note an antiferromagnetic character between the magnetization of Ti and Al on one side and those of Fe and Cr on the other side. The mBJ-GGA approach is reported to yield higher magnetization than that reported by the GGA. The direction of the interstitial magnetization coincides with that of the magnetization of Cr-3d and Fe-3d, except for the FeCrTiAs mBJ-GGA case. The total magnetic moment has the same direction in all Heusler alloys, which explain their ferrimagnetic comportment, according to the Slater-Pauling rule. The total magnetic moment increases proportionally with the increase in the total number of valence electrons. The Curie temperature T_C was estimated using the Mean Field Approximation (MFA), according to the following equation:

$$T_C = \frac{2}{3} \times \frac{\Delta E}{K_B} \tag{17}$$

Table 9 The spin magnetic moment (in Bohr magnetons μB) of the atoms constituting the Heusler alloys, the interstitial and total magnetic moments and Curie temperature T_C (in K) for FeCrTiM (M = Al, As, Si) calculated by GGA and mBJ-GGA approximations

		M_{Fe}	M_{Cr}	M_{Ti}	M_{Al}	M_{int}	M_{tot}	T_c
FeCrTiAl	GGA	0.612 0.626[7]	2.546 2.52[7]	−0.230 −0.246[7]	−0.024	0.09508	2.99 2.993[7] −2.99[8]	1548
	mBJ	0.635 0.65	2.567 2.89	−0.252 −0.38	−0.032	0.0825	3.00 3.00[10]	
FeCrTiAs	GGA	0.48231	0.69860	−0.17716	−0.01097	0.0007	0.993	406
	mBJ	0.536	0.765	−0.261	−0.022	−0.0176	1.00	
FeCrTiSi	GGA	0.61276 0.617[9]	1.53799 1.49942[9]	−0.18990 −0.187[9]	−0.02479 −0.02121[9]	0.06392 0.09088[9]	1.9998 1.99865[9]	770
	mBJ	0.683 0.648[9]	1.563 1.575[9]	−0.252 −0.252[9]	−0.041 −0.033[9]	0.046 0.062[9]	2.00 2.00[9] −1.99[8]	

where ΔE represents the energy difference between the ferrimagnetic and antiferromagnetic states, and k_B is the Boltzmann constant. The Curie temperature (T_C) of the FeCrTiM (M = Al, As, Si) compounds was calculated using the Mean Field Approximation (MFA), as shown in the Table 9. The results indicate that all the studied systems exhibit relatively high Curie temperatures, exceeding room temperature. Specifically, FeCrTiAl shows the highest T_C of approximately 1548 K, followed by FeCrTiSi and FeCrTiAs with values of 770 K and 406 K, respectively. These findings confirm the thermal stability of the ferrimagnetic behavior in these compounds and suggest their potential suitability for practical applications in spintronic and magnetic devices.

3.4.1 Slater–pauling rule and electronic configurations

For quaternary Heusler alloys, several variants of the Slater–Pauling rule have been reported, depending on the atomic arrangement and electronic hybridization. In particular, LiMgPdSn-type quaternaries can follow either Mtot = Ztot − 18 or Mtot = 24 − Ztot. Our calculations show that the compounds studied here (FeCrTiM, M = Al, Si, As) obey the latter relation:

$$M_{tot} = 24 - Ztot \tag{18}$$

where Ztott is the total number of valence electrons in the primitive cell. This rule applies to half-metallic Heusler alloys in which one spin channel exhibits metallic character while the other has a semiconducting gap. The total number of valence electrons Ztot is obtained from the electronic configurations of the constituent elements:

- **Fe**: [Ar] $3d^6\ 4s^2 \rightarrow 8$ valence electrons
- **Cr**: [Ar] $3d^5\ 4s^1 \rightarrow 6$ valence electrons
- **Ti**: [Ar] $3d^2\ 4s^2 \rightarrow 4$ valence electrons
- **Al**: [Ne] $3s^2\ 3p^1 \rightarrow 3$ valence electrons
- **As**: [Ar] $3d^1\ 4s^2\ 4p^3 \rightarrow 5$ valence electrons
- **Si**: [Ne] $3s^2\ 3p^2 \rightarrow 4$ valence electrons

Using these values:

- **FeCrTiAl**: $Z_{tot} = 8+6+4+3 = 21 \Rightarrow M_{tot} = 3\ \mu B$
- **FeCrTiAs**: $Z_{tot} = 8+6+4+5 = 23 \Rightarrow M_{tot} = 1\ \mu B$
- **FeCrTiSi**: Ztot = 8 + 6 + 4 + 4 = 22⇒Mtot = 2 μB

The calculated magnetic moments in Table 9 agree with this linear relationship, confirming the applicability of the Slater–Pauling behavior to these compounds.

3.5 Optical parameters

Optical parameters studied to illustrate the utility of these quaternary Heusler alloys include, real and imaginary dielectric constants, refractive index, imaginary dielectric tensor, extinction coefficient, energy loss, absorption coefficient, real optical conductivity and optical reflectivity are depicted in Fig. 11. The real part specifies the degree of polarization, indicates capacitive or inductive optical response of a material and it is more important in the visible region. The static dielectric constant refers to a sensitive property of a material, which indicates its ability to store electrical energy in low frequency. The static real dielectric constant for FeCrTiAl, FeCrTiSi and FeCrTiAs is 150, 75 and 55.The large static dielectric constant translates the high degree of polarization and points to the ferrielectric behavior of these materials. The real part of the dielectric function becomes negative between 3 and 6 eV. This explains that the electric displacement vector and the electric field vector point in the opposite directions. The combination between the lattice deformations, vibrational and strain dynamics contribute to the high static dielectric constant [45]. The imaginary part is associated with dielectric losses. The first peak of the imaginary dielectric tensor located in the energy

range between 0 and 1 eV corresponds to the drop of the real part of the dielectric function (Fig. 11). The refractive index is the measure of bending of a light ray when passing from one medium to another. It can also be defined as the ratio of the velocity of a light ray in an empty space to the velocity of light in a substance. The refractive index is an essential parameter in the design of photonic devices. Indeed, the high refractive index is a factor which limits the output efficiency of solar cells. The static refractive index for FeCrTiAl, FeCrTiSi and FeCrTiAs is 12, 8.4 and 7.5. The refractive index below 1 is observed at the ultraviolet photon energy and these materials become superluminal. The extinction coefficient is a characteristic that determines how strongly a species absorbs or reflects light at a particular wavelength. The static extinction coefficient for FeCrTiAl, FeCrTiSi and FeCrTiAs is 3, 2 and 1. When energy is converted to a different form, some of the input energy is turned into a highly disordered form of energy, and there is a loss energy. The loss energy is not important at visible and ultraviolet light for these quaternary Heusler under study. Prominent absorption peaks are observed in these compounds, which are polarized parallel to the chain axis *b*. The on-site Coulomb energies are estimated to be about 2.5 eV to 10 eV. When light absorption is more pronounced, this results in a decrease in light transmission. These materials exhibit large absorption coefficients in the visible and ultraviolet range located between $(100–170)\times10^4$ cm^{-1}. One can clearly recognize the strong absorption coefficient of 150 cm^{-1} for FeCrTiAl, FeCrTiSi and 170 cm^{-1} for FeCrTiAs at about 10 eV, which is ascribed to the infrared phonon mode. The high absorption coefficient at ultraviolet region, high reflectivity near infrared region, the narrow band gap semiconducting nature make these materials suitable for optoelectronic applications. The optical conductivity tensor characterizes the general linear heat conduction relation between temperature gradients and heat flux in heterogeneous anisotropic material. It is calculated for the Kohn–Sham energies and wave functions corresponding to the ground-state density. The conductivity tensor, σ(ω), derived from linear response theory, is:

$$\sigma(\omega)=\frac{ie^2}{3m^2\hbar\nu}\sum_k\sum_{nn'}\frac{f\left(\varepsilon_{nk}\right)-f\left(\varepsilon_{n'k}\right)\left|\Pi_{nn'}(k)\right|^2}{\omega_{nn'}(k)\omega-\omega_{nn'}(k)+i/\tau} \quad (19)$$

The real optical conductivity exhibits a prominent sharp peak at around 2.5 eV, 3 eV and 4 eV for FeCrTiAs, FeCrTiSi and FeCrTiAl. This peak was attributed to the transition from Fe, Cr and Ti orbitals to As, Si and Al orbital. Another peak appeared at about 9 eV for all these Heusler alloys. We note a reflectivity at zero frequency which is around 65 to 70% it gradually decreases until it disappears at 30eV.

3.6 Thermoelectric parameters

Spin-gapless semiconductors are a specific class of material; which band structure has an energy gap for a particular spin-orientation. The thermoelectric parameters are sensitive to spin state configurations, because energy differences are adopted in electronic transitions between orbits. Optimizing these materials requires enhancing their transport properties to maximize the so-called figure of merit. The figure of merit it is an essential element of the efficiency of a thermoelectric material for applications, which convert heat to electricity or, conversely, electric current to cooling. It is important to choose a material to simultaneously possesses a good electrical conductivity, high Seebeck coefficient, and a bad thermal conductivity. According to the Bardeen and Shockley deformation potential (DP) theory, the carrier relaxation time τ for acoustic phonon scattering is expressed as [46–48]:

$$\tau_{(sv)}=\frac{2(2\pi)^{1/2}\hbar^4C_l}{3\Xi^2\left(K_BT\right)^{3/2}\left(m_D^*\right)^{3/2}} \quad (20)$$

where $\hbar$ is the reduced Planck constant (1.055×10^{-34} J·s), C_l is the average elastic constant (GPa), k_B is Boltzmann's constant (1.381×10^{-23} J/K), T is the absolute temperature (K), m^* is the carrier effective mass (kg), and Ξ is the acoustic deformation potential (eV).

For cubic crystals, the longitudinal elastic constant is taken as:

$$C_l=\frac{C_{11}+2C_{44}}{3} \quad (21)$$

In the present calculation, we used room temperature T = 300 K, an effective mass $m^*\approx0.5m_0=4.55\times10^{-31}$ kg (typical for Heusler alloys), and a deformation potential Ξ = 10 eV (typical for transition-metal compounds). The computed values of the relaxation time τ for the studied compounds are summarized in Table 10.

Figure 12; illustrates the effect of chemical potential shifted with respect to the Fermi energy from −2 eV to 2 eV on Seebeck coefficient (a), electrical conductivity (b), electronic thermal conductivity (c) and figure of merit (d), using mBJ –GGA for spin-up and spin-down at 300

Table 10 Calculated average elastic constants and carrier relaxation times τ\tauτ at 300 K

Compound	Average Elastic Constant (GPa)	Relaxation Time τ (s)
FeCrTiAl	162.5	1.24×10^{-14}
FeCrTiAs	135.1	1.03×10^{-14}
FeCrTiSi	166.7	1.27×10^{-14}

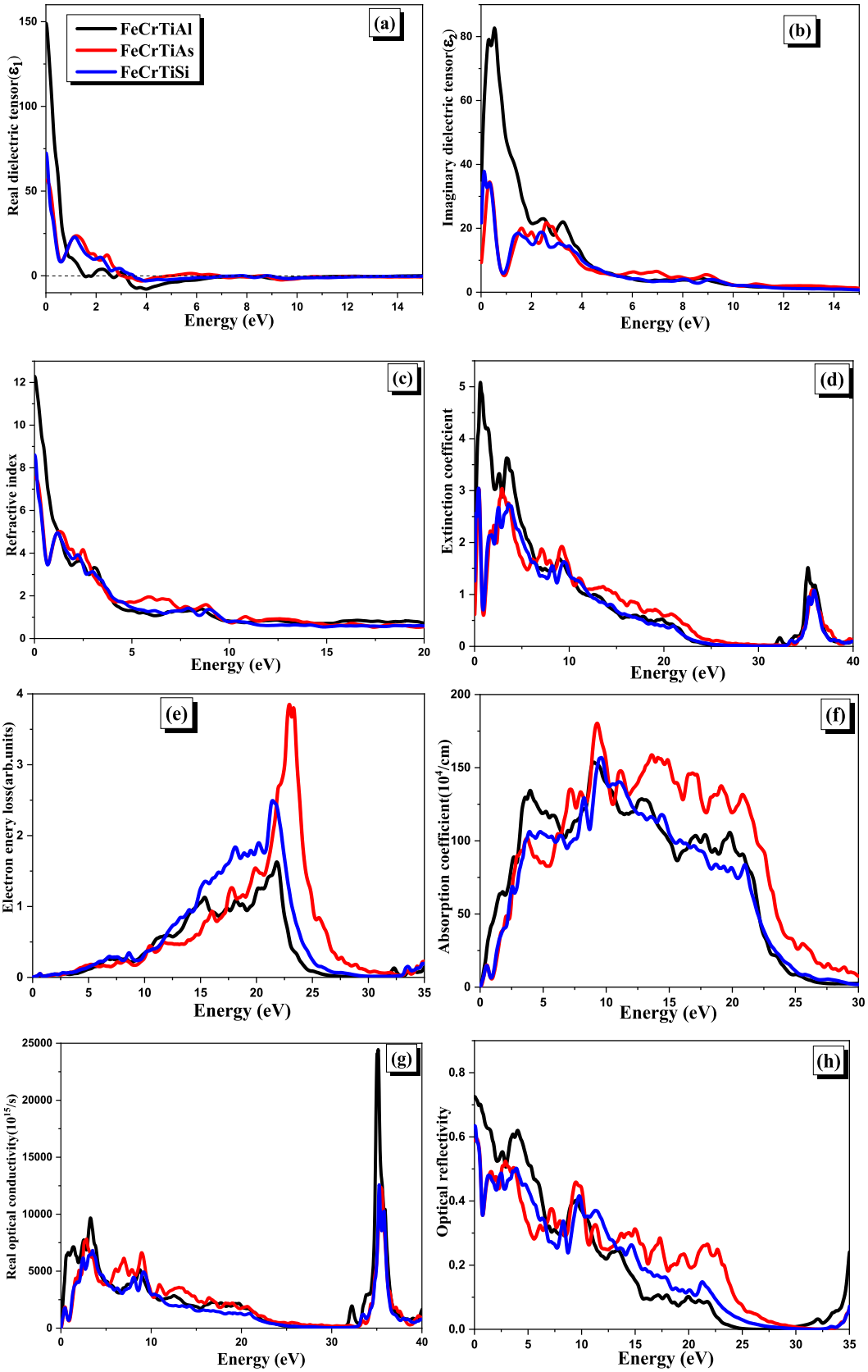
(a)
FeCrTiAl
FeCrTiAs
FeCrTiSi
Real dielectric tensor(ε1)
Energy (eV)
(b)
Imaginary dielectric tensor(ε2)
Energy (eV)
(c)
Refractive index
Energy (eV)
(d)
Extinction coefficient
Energy (eV)
(e)
Electron enery loss(arb.units)
Energy (eV)
(f)
Absorption coefficient(10^4/cm)
Energy (eV)
(g)
Real optical conductivity(10^15/s)
Energy (eV)
(h)
Optical reflectivity
Energy (eV)

◂**Fig. 11** Variation in the following properties as a function of photon energy for FeCrTiAl, FeCrTiAs, and FeCrTiSi compounds based on the mBJ-GGA approximation: **a** real part of the dielectric function, **b** imaginary part of the dielectric function, **c** refractive index, **d** extinction coefficient, **e** energy loss function, **f** absorption coefficient, **g** real optical conductivity, and **h** optical reflectivity

K. Seebeck coefficient increases with increasing chemical potential. For the spin-up (spin-dn), there is one peak in the profile around 0.25 eV (0.75 eV) for p-type (n-type) charge carriers. The calculated Seebeck coefficients at 300 K reach up to ~ 1350 $\mu V \cdot K^{-1}$ for FeCrTiSi, ~ 1250 $\mu V \cdot K^{-1}$ for FeCrTiAs, and ~ 750 $\mu V \cdot K^{-1}$ for FeCrTiAl in the spin-up channel. In the spin-down channel, the maximum values are approximately − 1500 $\mu V \cdot K^{-1}$, − 1500 $\mu V \cdot K^{-1}$, and − 1000 $\mu V \cdot K^{-1}$, respectively. The predicted figure of merit (ZT) approaches ~ 1 near the Fermi level for both carrier types and both spin channels at 300 K. The p-type behavior is ensured by positive charge carriers, as confirmed by the positive Seebeck coefficient. The n-type behavior results from asymmetric band structures. At low temperatures (300 K), carrier mobility is high, leading to a high Seebeck coefficient. At 300 K, efficient n-type thermoelectric materials are expected to exhibit large electrical conductivity. In our calculations, the maximum value of (σ/τ) is $\sim 3.5 \times 10^{20}\ \Omega^{-1} \cdot m^{-1} \cdot s^{-1}$ for p-type carriers. Assuming a typical relaxation time $\tau \approx 10^{-14}$ s, this corresponds to $\sigma \approx 3.5 \times 10^{6}\ S \cdot m^{-1}$ $(\Omega^{-1} \cdot m^{-1})$. Such a value indicates potential applicability for thermoelectric conversion in both spin channels. Phonon scattering arising from lattice vibrations and defects is expected to reduce the lattice contribution to the thermal conductivity, thereby enhancing ZT. The total thermal conductivity is the sum of electronic and lattice parts. The calculated $(k/\tau) \approx 2.5 \times 10^{15}\ W \cdot m^{-1} \cdot K^{-1} \cdot s^{-1}$ yields an estimated electronic thermal conductivity of ~ 25 $W \cdot m^{-1} \cdot K^{-1}$, which lies in the range typically considered favorable for thermoelectric performance. A figure of merit is a parameter used to characterize the performance of a device system. The figure of merit (ZT) is the most widely used descriptor for evaluating the efficiency of a thermoelectric material. In this case, the figure of merit is symmetric with respect to the energy $E - E_F = 0.25$. The maximum figure of merit value is ≈1 obtained around the Fermi level for both type carriers and both spin at 300 K. Heusler compounds spin-gapless semiconductors materials with adequate structure lead to an improvement of the figure of merit of ~ 1. Studies of FeCrTiSi, FeCrTiAs and FeCrTiAl should lead to a real potential of using thermoelectricity for large scale applications. The predicted high electrical conductivity, low electronic thermal conductivity, and figure of merit (ZT ~ 1) for FeCrTiM (M = Al, As, Si) are highly competitive compared to other reported Heusler alloys, such as Co2TiSi and Fe2VAl, which typically exhibit lower ZT values [49, 50]. Figure 13; shows the effect of temperature on lattice thermal conductivity (a), electronic thermal conductivity (b), total thermal conductivity (c), electrical conductivity via relaxation time (σ/τ) (d), Seebeck coefficients (e) and figure of merit (f) for FeCrTiAl, FeCrTiAs, and FeCrTiSi. The lattice component of thermal conductivity refers to the conduction of heat by the vibrations of lattice ions in a material. We note that the lattice thermal conductivity is not sensitive to the temperature for FeCrTiAl and FeCrTiAs, but it decreases monotonously with increasing temperature for FeCrTiSi. Electronic thermal conductivity involves the transfer of thermal energy by a combination of diffusion of electrons and phonon vibrations. Thermal electronic conductivity is not affected at low temperatures. At high temperatures growth is parabolic. The total thermal conductivity as a function of temperature follows that of lattice thermal conductivity. Electrical conductivity is a measure of the ability of the material to conduct an electrical current. FeCrTiSi electrical conductivity is not sensitive to temperature, while that of FeCrTiAl and FeCrTiAs follows a parabolic vanishing. Compared to similar Heusler alloys materials, these compounds exhibit competitive thermoelectric performance with ZT values ≈ 1, high Seebeck coefficients (up to 1500 μV/K), good electrical conductivity $(3.5 \times 10^{6}\ (\Omega ms)^{-1})$, and relatively low electronic thermal conductivity (25 $W(mKs)^{-1}$). The spin-gapless semiconductor behavior of FeCrTiAs and FeCrTiSi provides a unique advantage in enhancing the power factor $(S^2\sigma)$, although future challenges include improving thermal stability and mechanical properties for practical applications.

4 Conclusion

The optimized lattice constants and bulk modulus performed on FeCrTiAs and FeCrTiAl is predictions. Structural, mechanical, thermodynamic and dynamic stabilities are present in all Heuslers under study. The optical mode in the studied Heusler alloys is mainly due to the vibrations of Al, Cr and Si (Fe and Ti) atoms in opposite direction (same direction). The upper valence band is due to the orbits of Fe and Cr for both spins and we observe a hybridization of the Fe, Cr and Ti states. The analysis of Poisson's ratio values indicates no microstructural deformation ($\nu > 0$) in all compounds. FeCrTiAs and FeCrTiSi exhibit metallic bonding ($\nu \geq 0.33$), whereas FeCrTiAl shows a lower value ($\nu = 0.25$), indicative of a more covalent character. The quaternary Heusler alloys under study obey to the Slater-Pauling rule, where the origin is explained in terms of orbitals hybridization. Local octahedral coordination of Fe (3d), Cr (3d) and Ti (2d) atoms in FeCrTiAl for both spin gives two degenerate orbitals. The anti-bonding states

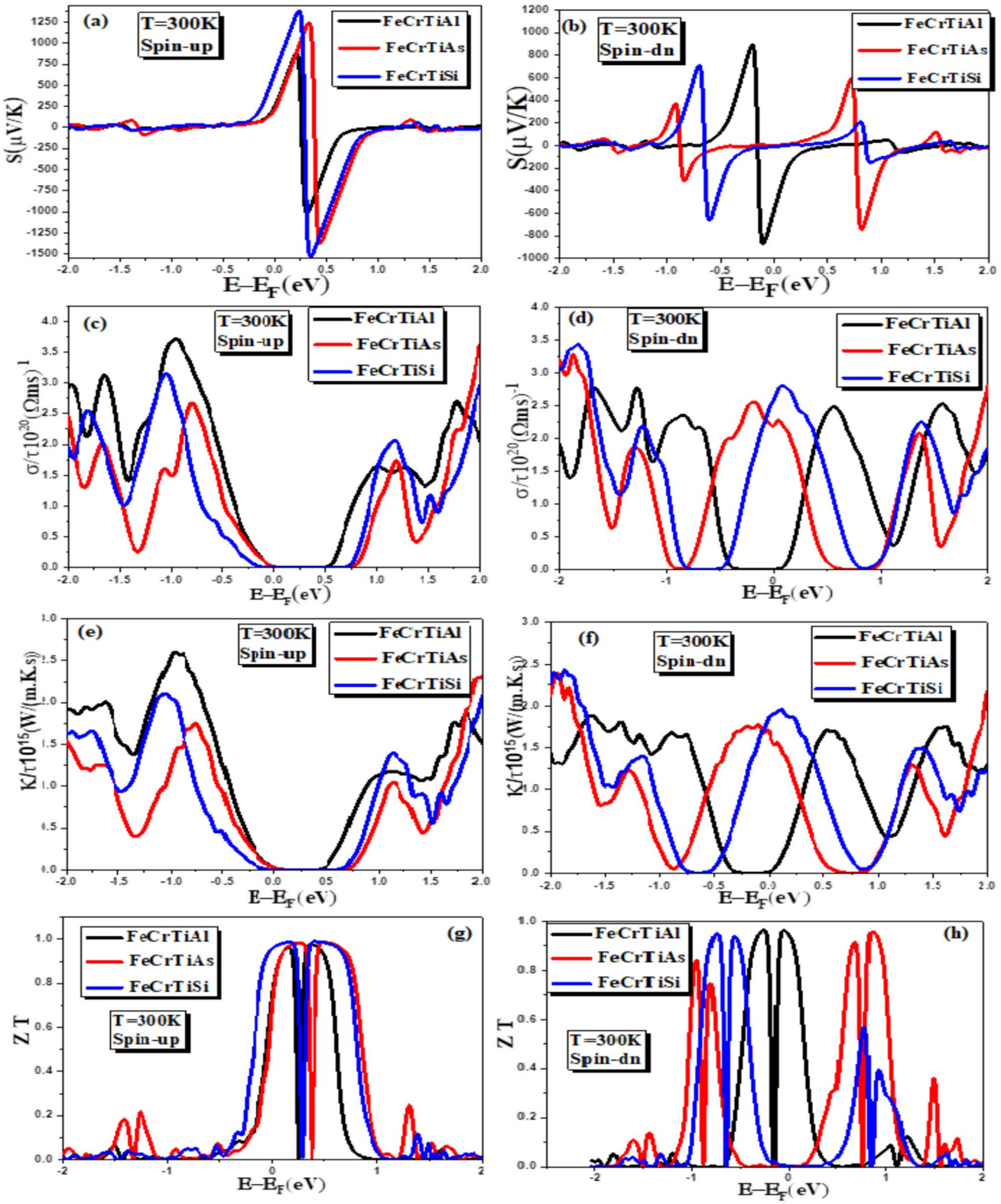

Fig. 12 The Seebeck coefficient **a**, **b**, Electrical conductivity **c**, **d**, Electronic thermal conductivity **e**, **f**, figure of merit **g**, **h** as a function of chemical with (spin-up and spin-down states) using GGA–mBJ potential

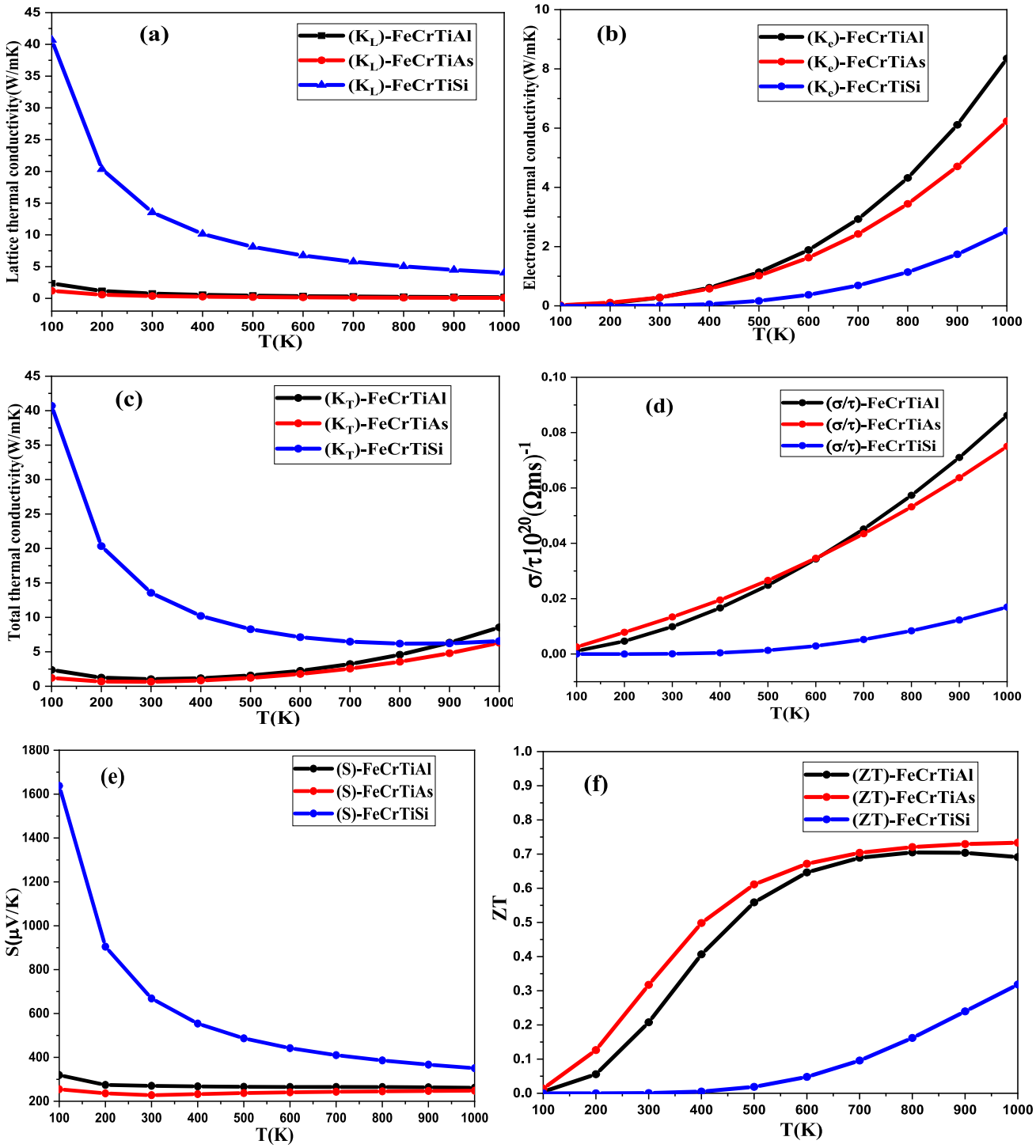

Fig. 13 Temperature sensitivity of various properties for FeCrTiAl, FeCrTiAs, and FeCrTiSi compounds based on mBJ-GGA approximation: **a** lattice thermal conductivity (K_L), **b** electronic thermal conductivity (K_e), **c** total thermal conductivity (K_T), **d** electrical conductivity via relaxation time (σ/τ), **e** Seebeck coefficients (S) and **f** figure of merit (ZT)

(Fe, Cr, Ti)—(Si, Al, As) and no zero PDOS near the Fermi level for both spins reduce the energy of the occupied states eg, which have lower energy than the t2g, this explains the metallic character of the Heuslers studied. All Heuslers exhibit ferrimagnetic character with major contribution to the magnetization comes from the unfilled Fe-3d and Cr-3d orbitals. The large static dielectric constant translates the high degree of polarization and points to the ferrielectric behavior of these

materials. The high absorption coefficient in the ultraviolet region, the high reflectivity in the near infrared region, and the narrow band gap semiconducting character suggest that these materials could be promising for optoelectronic applications, pending experimental validation. This study is entirely based on first-principles DFT calculations. While the results provide valuable predictions of structural, electronic, magnetic, optical, and thermoelectric properties, they may not fully capture synthesis challenges, intrinsic defects, or finite-temperature effects. Experimental validation is therefore required to confirm the predicted half-metallicity, transport coefficients, and stability under realistic operating conditions.

Acknowledgements The authors extend their appreciation to the Deanship of Scientific Research at Northern Border University, Arar, KSA for funding this research work through the project number NBU FPEJ-2025-310-01

Authors contribution Conceptualization: K.Bouferrache, R. Ameur, A. Guibadj Data curation: M.A. Ghebouli Formal analysis: B. Ghebouli Validation: M. Fatmi, Faisal Katib alanazi.

Funding The authors extend their appreciation to the Deanship of Scientific Research at Northern Border University, Arar, KSA for funding this research work through the project number NBU-FPEJ-2025–310-01.

Data availability Data underlying the results presented in this paper are not publicly available at this time but may be obtained from the author (fatmimessaoud@yahoo.fr) upon reasonable request.

Declarations

Conflicting interests The authors declared no potential conflicts of interest.

Competing interests The authors declare no competing interests.

References

1. Graf T, Felser C, Parkin SSP (2011) Simple rules for the understanding of Heusler compounds. Prog Solid State Chem 39(1):1–50
2. Felser C, Wollmann L, Chadov S, Fecher GH, Parkin SSP (2015) Basics and prospective of magnetic Heusler compounds. APL Mater 3(4):041518
3. Galanakis I, Mavropoulos P, Dederichs PH (2023) Electronic structure and Slater-Pauling behaviour in half-metallic Heusler alloys. Inorg Chem Commun 150:110479
4. Hebri S, Abdelli A-B, Belfedal N, Bensaid D (2020) Investigating the structural, electronic, and elastic properties of Li-based quaternary Heusler alloy semiconductors using hybrid functional – HSE06 bandgap recalculations. J Alloys Compd 822:153633
5. Slater JC (1936) The ferromagnetism of nickel. II. Temperature effects. Phys Rev 49(12):931
6. Özdoğan K, Šašıoğlu E, Galanakis I (2013) J Appl Phys 113:193903. https://doi.org/10.1063/1.4805063
7. Pavel Lukashev V, Stephen MC, Paul Shand M, Parashu K (2023) J Magnet Magnet Mater 584:171107
8. Dhakal R, Nepal S, Galanakis I, Adhikari RP, Kaphle GC (2021) Prediction of half-metallicity and spin-gapless semiconducting behavior in the new series of FeCr-based quaternary Heusler alloys: An Ab initio study. J Alloys Compd 882:160500. https://doi.org/10.1016/j.jallcom.2021.160500
9. Hebri S, Abdelli A, Belfedal N, Bensaid D (2023) Inorg Chem Commun 150:110479. https://doi.org/10.1016/j.inoche.2023.110479
10. Alijani V, Ouardi S, Fecher GH, Winterlik J, Naghavi SS, Kozina X, Stryganyuk G, Felser C (2011) Electronic, structural, and magnetic properties of the half-metallic ferromagnetic quaternary Heusler compounds CoFeMn<mml:math xmlns:mml="http://www.w3.org/1998/Math/MathML" display="inline"><mml:mi>Z</mml:mi></mml:math>(<mml:math xmlns:mml="http://www.w3.org/1998/Math/MathML" display="inline"><mml:mrow><mml:mi>Z</mml:mi><mml:mo>=</mml:mo><mml:mtext>Al</mml:mtext></mml:mrow></mml:math>, Ga, Si, Ge). Phys Rev B 84:224416. https://doi.org/10.1103/PhysRevB.84.224416
11. Quyoom Seh A, Gupta DC (2021) Quaternary Heusler alloys a future perspective for revolutionizing conventional semiconductor technology. J Alloys Compd 871:159560. https://doi.org/10.1016/j.jallcom.2021.159560
12. Idrissi S, Labrim H, Ziti S, Bahmad L (2021) A DFT study of the equiatomic quaternary Heusler alloys ZnCdXMn (X=Pd, Ni or Pt). Solid State Commun 331:114292. https://doi.org/10.1016/j.ssc.2021.114292
13. Bainsla L, Suresh KG (2016) Equiatomic quaternary Heusler alloys: A material perspective for spintronic applications. Appl Phys Rev 3:031101. https://doi.org/10.1063/1.4959093
14. Kundu A, Ghosh S, Banerjee R, Ghosh S, Sanyal B (2017) Sci Rep 7:1803. https://doi.org/10.1038/s41598-017-01782-5
15. Prakash R, Gopalakrishnan P (2023) RSC Adv 13(16):10847. https://doi.org/10.1039/d3ra00942d
16. Galanakis I (2023) Nanomaterials 13(13):2010. https://doi.org/10.3390/nano13132010
17. Kaur N, Sharma R, Srivastava V, Chowdhury S (2023) Thermodynamic and thermoelectric properties of FeCrTiZ (Z = Si, Ge) quaternary Heusler compounds. J Chem Thermodyn 184:107089. https://doi.org/10.1016/j.jct.2023.107089
18. Klinton Brito K, Shobana Priyanka D, Srinivasan M, Sudharsan JB, Fujiwara K, Ramasamy P (2024) Skutterudites as sustainable thermoelectric material- A critical review. Solid State Sci 157:107721. https://doi.org/10.1016/j.solidstatesciences.2024.107721
19. Brito KK, Priyanka DS, Srinivasan M, Ramasamy P (2024) First principle investigations on structural, mechanical, electronic, and thermoelectric properties of XCoP (X2Ti, Zr, Hf) half Heusler

alloys for energy recovery application. Cryst Res Technol. https://doi.org/10.1002/crat.202300181
20 Beenaben S, Sankararajan R, Srinivasan Manickam K (2025) KlintonBrito, An ab initio study on semiconducting half Heusler alloys TiAgZ (Z=Al, Ga, In) for thermoelectric and optoelectronic applications. Mater Sci Semiconduct Process 189:109251. https://doi.org/10.1016/j.mssp.2024.109251
21 Beenaben SS, Sankararajan R, Srinivasan Manickam A, Klinton-Brito K, Prasath M (2025) MnNiSi Half-Heusler Alloy: Computational and experimental insights for energy harvesting and spintronic applications. Chem Phys Impact 10:100891. https://doi.org/10.1016/j.chphi.2025.100891
22. Balasubramanian S, Priyanka S, Manickam S, Brito K, Eswaramoorthy N, Bojarajan AK, Sangaraju S (2024) An ab initio investigation on $BaXO_3$ (X = Cr, Mn, Sc) oxide perovskites for spintronic applications. New J Chem 48:14213–14224. https://doi.org/10.1039/D4NJ02421D
23. Blaha P, Schwarz K, Madsen GKH, Kvasnicka D (2001) WIEN2k: an augmented plane wave plus local orbitals program for calculating crystal properties
24. Ghebouli MA, Bouferrache K, Alanazi FK, Ghebouli B, Fatmi M (2025) Computational Insights into the Stability, Mechanical, Optoelectronic, and Thermoelectric Characteristics Investigation on Lead-Based Double Perovskites of (Cs2, K2, Rb2)PbCl6: Promising Candidates for Optoelectronic Applications. Adv Theory Simul 8(3):2400938. https://doi.org/10.1002/adts.202400938
25. Burke K, Perdew JP, Ernzerhof M (1998) Why semilocal functionals work: Accuracy of the on-top pair density and importance of system averaging. J Chem Phys 109(10):3760–3771
26. Xiang HJ, Singh DJ (2007) Phys Rev B 76:195111
27. Slack GA (1973) Nonmetallic crystals with high thermal conductivity. J Phys Chem Solids 34:321–335
28. Berman R, Klemens PG (1978) Thermal conduction in solids. Phys Today. https://doi.org/10.1063/1.2994996
29 Julian CL (1965) Theory of Heat Conduction in Rare-Gas Crystals. Phys Rev 137:128–37
30. Galanakis I, Özdoğan K, Şaşıoğlu E, Aktaş B (2014) Structural, electronic, and magnetic properties of quaternary Heusler alloys. Phys Rev B 89(22):224408
31. Hebri S, Boukhlifi F, Boukhris S (2020) First-principles study of structural, electronic, and magnetic properties of lithium-based quaternary Heusler alloys. J Magn Magn Mater 500:166408
32. Murnaghan FD (1944) Proceeding National Academy of Sciences USA, 30, 244-247
33 Klinton Brito K, Shobana Priyanka D, Srinivasan M, Ramasamy P (2024) Ferrimagnetic half metals TaMnZ (Z = As, Sb, Bi) for thermoelectric and spintronic applicationsMaterial computations. J Magnet Magnetic Mater 610:172564. https://doi.org/10.1016/j.jmmm.2024.172564
34. Klinton Brito K, Sudharsan JB, Srinivasan M, Prammitha R, Prasath M, Nivetha GF (2025) Hafnium based ferromagnetic half metals for spintronic and thermoelectric applications Materials Computation. Comput Theor Chem 1246:115124. https://doi.org/10.1016/j.comptc.2025.115124
35. Klinton Brito K, Sudharsan JB, Srinivasan M, Ramasamy P (2024) Alkali-based half metals as sustainable materials for spin electronics and energy harvesting application Materials computation. Comput Theor Chem 1241:114871. https://doi.org/10.1016/j.comptc.2024.114871
36. Born M, Huang K (1954) Dynamical Theory of Crystal Lattices. Oxford University Press
37. Monir MEA, Reguig AB, Ghebouli MA, Bouferrache K, Alanazi FK, Fatmi M, Bouandas H (2025) Structural, elastic, electronic, magnetic and thermal properties of X_3FeO_4 (X = Mg, Ca and Sr) materials. Sci Rep 15:2957. https://doi.org/10.1038/s41598-025-87466-x
38. Voigt W (1928) Lehrbuch der Kristallphysik. Teubner, Leipzig
39. Reuss A, Angew Z (1929) Math Mech 9:49. https://doi.org/10.1002/zamm.19290090104
40. Hill R (1952) Proc Phys Soc A 65:349. https://doi.org/10.1088/0370-1298/65/5/307
41. Hill R, Mech J (1963). Phys Solids 11, 357.https://doi.org/10.1016/0022-5096(63)90036-X
42. Pugh SF (1954) Relations between the elastic moduli and the plastic properties of polycrystalline pure metals. Philos Mag 45(367):823–843
43. Wang XL, Sui Y, Cheng ZX (2016) Spin gapless semiconductors and their applications. J Appl Phys 119(2):025104
44. Ghebouli MA, Bouferrache K, Alanazi FK, Ghebouli B, Fatmi M (2025) Computational insights into the stability, mechanical, optoelectronic, and thermoelectric characteristics investigation on lead-based double perovskites of (Cs2, K2, Rb2)PbCl6: promising candidates for optoelectronic applications. Adv Theory Simul 8(3):2400938
45. Guo H, Baker JS, Wu W, Choy KL (2023) High Dielectric Constants in BaTiO3 Due to Phonon Mode Softening Induced by Lattice Strains: First Principles Calculations. Adv Phys Res 2(9):2300001
46. Klinton Brito K, Shobana Priyanka D, Srinivasan M, Ramasamy P (2024) Computations on platinum based ternary ferromagnetic half metals for spin valve diodes and green energy technology based thermoelectric. J Magn Magn Mater 589:171629. https://doi.org/10.1016/j.jmmm.2023.171629
47. Klinton Brito K, Jai Muthukumaran J, Srinivasan M (2025) First-principles calculations on structural, elastic, electronic, magnetic and thermoelectric properties of hafnium-based ferrimagnetic half metals. J Magnet Magnet Mater 629:173296. https://doi.org/10.1016/j.jmmm.2025.173296
48. Liu J, Jiang QY, Zhang S, Zhang H (2019) Carrier mobility and relaxation time in BiCuSeO. Phys Lett A 383(34):125990. https://doi.org/10.1016/j.physleta.2019.125990
49. Sakurada S, Shutoh N (2005) Effect of Ti substitution on the thermoelectric properties of (Zr,Hf)NiSn half-Heusler compounds. Appl Phys Lett 86(8):082105
50. Bhattacharya S, Madsen GKH, Singh DJ (2016) Thermoelectric properties of Heusler alloys. J Appl Phys 119(2):025104